DEFORMATION OF THE EASTERN CORDILLERA, NW ARGENTINA

Kinematics and mechanisms of upper-crustal deformation in the Eastern Cordillera, southern Central Andes, NW Argentina

by
Tasca Noela Santimano

A Thesis
presented to the School of Geography and Earth Sciences
in conformity with the requirements
for the Degree of
Master of Science

McMaster University
Hamilton, Ontario
December, 2010

© Copyright by Tasca Noela Santimano, 2010

MASTER OF SCIENCE (2010) McMaster University

School of Geography and Earth Sciences Hamilton, Ontario

TITLE: Kinematics and mechanisms of upper-crustal deformation in the Eastern Cordillera, southern Central Andes, NW Argentina

AUTHOR: Tasca Noela Santimano

SUPERVISOR: Prof. Dr. Ulrich Riller

NUMBER OF PAGES: ii, 57

Abstract

The Puna Plateau is the second highest continental plateau on Earth and is bordered by the Eastern Cordillera to the east. The growth of this plateau in a non-collisional tectonic setting is not well understood and requires an understanding of the deformation mechanisms and kinematics of its margins, notably the Eastern Cordillera. Deformation in the Eastern Cordillera is characterized by basement-involved folding and reverse faulting during the Tertiary and Quaternary. However, the orientation and kinematics of first-order structural elements of the Eastern Cordillera are not well known. This is addressed in this thesis by a comprehensive structural analysis of three key areas, La Poma, Southern Luracatao Valley and Cachi, in the Eastern Cordillera. Specifically, my structural analyses encompassed (1) field mapping and remote sensing of first-order fold structures and faults, (2) 3D modelling of these structures and (3) a detailed analysis of small-scale brittle shear faults (828 faults at 79 stations). Examination of first-order structures revealed that the Eastern Cordillera was affected by two deformation regimes: Non-cylindrical deformation, i.e., doming of upper crust, followed by cylindrical deformation, notably formation of km-scale folds with straight hinge lines in the hanging walls of orogen-parallel thrust and reverse faults. 3D modelling of these faults at La Poma and Luracatao Valley in the Eastern Cordillera revealed that west-dipping faults are consistently shallower than east-dipping ones. Displacement on shallow (< 15°) west-dipping thrust faults in the La Poma area amounts to 2.4 km and likely exceeds displacement magnitudes on east-dipping reverse faults. Analysis of brittle shear faults indicates that doming occurred during E-W shortening. This was followed by NE-SW-shortening on west-dipping thrust and reverse faults and later by NW-SE shortening on east-dipping reverse faults, which induced also a component

of left-lateral displacement on N-S striking reverse faults. Brittle fault analysis indicates that shortening directions vary greatly in space and time and seem to depend rather on the local kinematic regime of first-order structures (domes, thrusts and reverse faults) than on far-field stresses related to plate boundary forces. Collectively, the structural analysis suggests that deformation was controlled by the local structural complexity of upper crust, including higher-order, pre-Andean mechanical anisotropies (such as aplitic dikes, foliation surfaces and cretaceous normal faults).

I dedicate this thesis to my parents

Virginia and Samson Santimano

Acknowledgement

Achieving the goal of completing my Masters degree would not be possible without the guidance of my advisor and mentor Ulrich Riller. He always believed in me, took me out of my shell and showed me what I am capable of producing. I thank him for all his advice and support.

I would like to thank Fernando Hongn, Ivan Petrinovic and Silvina Guzmán for introducing me to the Central Andes. I would also like to thank Silvina Guzmán for showing me Argentina and taking care of me like a sister. Many thanks to Guadalupe Zarzoso for assisting me during my first field season, Patricio Bosio for sharing his knowledge of the Luracatao Valley, Heidi Daxberger for assisting me in the field during my second field season. I must also thank all the people in Salta and in the Calchaquí Valley and Luracatao Valley for taking care of me, providing me with a roof to sleep under and patiently listening to my broken Spanish with a big smile. Thank you also to Bill Morris for providing a license of Geomodeller for all the 3D models.

Thank you to my good friend Sharon Sequeira for supporting me during the course of the last two years, Nicola Martis for telling me that I can write my thesis in 6 hours and for giving me a game plan. It took a lot longer than that but the teacher in her helped me start the writing process and Martin Clark for all the motivational talks and early morning laughs in the lab.

Lastly, I would like to thank my Parents, my Mom for listening to me with a patient ear and tolerating my mood while I wrote my thesis, my Dad for always taking an interest in what I did and for making a wish 25 years ago, that I become a Geologist and my brother Rahul for always supporting me and encouraging me to do better things in life. To my Parents and my brother I owe the person I am.

Table of Contents

List of Figures

List of Tables

Chapter 1: Introduction

The Puna Plateau in the Central Andes (Fig. 1a) is the second highest continental plateau on Earth and formed by E-W lithospheric shortening since Eocene-Oligocene times (Isacks, 1988; Allmendinger et al., 1997). In detail, however, the formation of this plateau in a non-collisional tectonic setting, located hundreds of kilometres east of the plate boundary, is not well understood. For example, the orientation and kinematic history of first-order structural elements, notably reverse faults, in the Puna and the adjacent Eastern Cordillera (Fig. 1b) are unknown. Moreover, deformation on the Puna Plateau and Eastern Cordillera has been related to a change in convergence parameters of the subducting plate (Oncken et al., 2006). However, it is uncertain how and to what extent plate boundary forces are transmitted to the Puna and the Eastern Cordillera. For example, analyses of brittle faults suggested that a phase of thrusting under NW-SE horizontal shortening and subvertical extension during the Miocene and Pliocene was apparently followed by a phase of strike-slip deformation under NE- SW shortening in the Puna and the Eastern Cordillera during the Pliocene and Quaternary (Marrett et al., 1994). The change in the shortening directions has been related to the change in the direction and rate of absolute motion of the South American Plate (Marrett and Strecker, 2000). Alternatively, the two shortening directions are interpreted to have occurred largely simultaneously and related to the segmentation of the upper crust into rhomb-shaped basins rimmed by sigmoidal transpressive deformation zones (Riller & Oncken, 2003).

Understanding the kinematics of deformation that controls the formation of prominent structures is important for understanding the tectonic evolution of the Eastern Cordillera. The objective of

the study is, therefore, to conduct a comprehensive structural analysis in selected areas of the Eastern Cordillera to better understand the kinematics of deformation at the eastern margin of the Puna Plateau (Fig. 1b). Specifically, the geometry of first-order fault planes is identified, through field mapping, remote sensing techniques and 3D modelling is identified, in order to constrain the mechanisms of upper-crustal deformation. Moreover, fault-slip data are used to elucidate principal paleo-stress directions of the upper crust and, by inference, the sense of displacement on first-order faults and history of deformation phases in the Eastern Cordillera.

Analysis of the fault-slip data shows that shortening directions are dependent on the local geological setting. Results from the combination of field work, analysis of brittle fault-slip data, 3D modelling and remote sensing of the three areas provides a history of the deformation mechanism. The areas chosen for this study were based on the structural inventory and excellent exposure of prominent structures. The areas are, (1) La Poma in the northern Calchaquí Valley, (2) the southern part of the Luracatao Valley and (3) Cachi in the center of the Calchaquí Valley (Fig. 1c). Because of their proximity to the Puna, the study areas in the Calchaquí Valley and the Luracatao Valley are of particular structural interest.

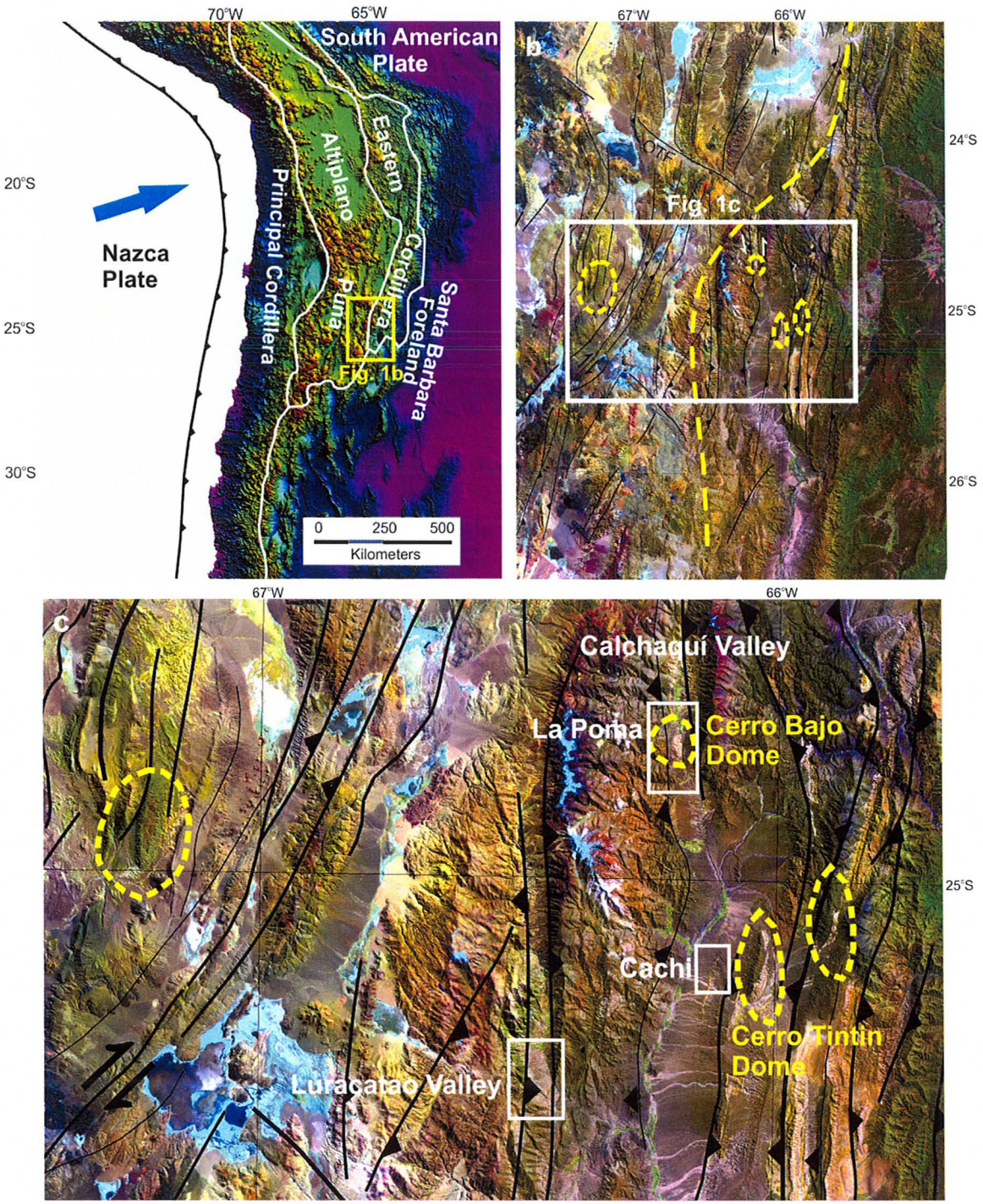

Figure 1- Geological setting of the study area. (a) Morphotectonic units of the Central Andes (modified from Strecker et al., 2007). (b) Satellite TM scene showing the Puna Plateau and the Eastern Cordillera indicating the presence of domes (yellow circles) and first-order faults (black lines). Yellow stippled line delineates the boundary based on the 3000m elevation between the Puna Plateau to the west and the Eastern Cordillera to the east. (c) Satellite TM scene showing the three study areas in the Calchaquíes Valleys.

Chapter 2: Geological Setting

The structural study focuses on areas of the Eastern Cordillera of the Central Andes which is located between the Puna Plateau to the west and the thin-skinned Santa Barbara foreland fold-and-thrust belt to the east (Fig. 1a). These morphotectonic regions formed due to horizontal shortening of the upper plate, the South American Plate, imparted by convergence and eastward subduction of the oceanic Nazca plate (Isacks, 1988). Deformation in these regions commenced in Eocene times and propagated eastward (Mon & Salfity, 1995; DeCelle and Horton, 2003; Deeken et al., 2006). Shortening was accomplished by distributed deformation in the Puna, whereas localized basement-involved folding and thrusting is more typical for the Eastern Cordillera (Kley, 1996; Kley et al., 1996, 1997). Horizontal shortening led in both regions to formation of N-S trending compressional basins and morphological ranges (Fig. 1b). However, the Puna is characterized by a lower relief than the Eastern Cordillera (Isacks, 1988).

With an average elevation of about 3700 m, the Puna is about 1000 m lower than the average elevation of the Eastern Cordillera (Fig. 1a; Gephart, 1994). Thus, the Eastern Cordillera forms an orographic barrier to the Puna and thus prevents moist easterly winds from the eastern foreland to reach the plateau (Vandervoort et al., 1995; Strecker et al., 2007; Bookhagen and Strecker, 2008). Basins in the Puna are internally drained and generally wider than the valleys in the Eastern Cordillera. Arid climatic conditions since at least the mid Miocene led to accumulation of considerable salt deposits that are intercalated with clastic sedimentary strata in the closed basins of the Puna (Alonso et al., 1991; Vandervoort et al., 1995). Uplift of the ranges bordering the basins was accomplished on N-S striking, mostly sinistral oblique reverse faults

and NE-striking dextral oblique reverse faults (Fig. 1b; Riller and Oncken, 2003). Shortening affected also the basins, the strata of which were folded during Pliocene times (Marrett et al., 1994). Prominent NW-striking fault zones on the plateau are also associated with Neogene volcanic centers (Viramonte et al., 1984; Riller et al., 2001).

The Eastern Cordillera consists mainly of low-grade metamorphic basement rocks of the Late Neoproterozoic to Early Cambrian Puncoviscana Formation (Turner, 1960) and syntectonic Ordovician granitoid plutons (Fig. 2; Hongn and Riller, 2007). These rocks are unconformably overlain by Cretaceous and Tertiary sedimentary rocks of the Salta Group (Fig. 2). This Group is made up of the Pirgua, Balbuena and the Santa Barbara Subgroups, which formed during a phase of continental rifting prior to Andean orogenesis. The Pirgua Formation consists of coarse-grained syn-rift deposit at the base to well-sorted conglomerate and sandstone toward the top. The Balbuena group marks the post-rift phase and includes conglomerate and coarse-grained sandstone of the Lecho Formation and overlying dolomite of the Yacoraite Formation (Fig. 2; Blasco & Zapettini, 1995). The Santa Barbara Subgroup consists of sandstone and conglomerate of the Mealla and Maiz-Gordo Formations and is overlain unconformably by the Quebrada de los Colorados Formation of the Eocene to Neogene Payogastilla Subgroup (Fig. 2; Hongn et al., 2007). Fluvial and alluvial pediments of Quaternary age overlay in turn unconformably deformed Cretaceous and Tertiary strata. These strata are mostly preserved in the valleys, whereas Paleozoic basement rocks that are thrust over these strata make up the ranges. As a consequence, Quaternary pediments consist mainly of boulders of Puncoviscana Formation and Ordovician granitoid rocks.

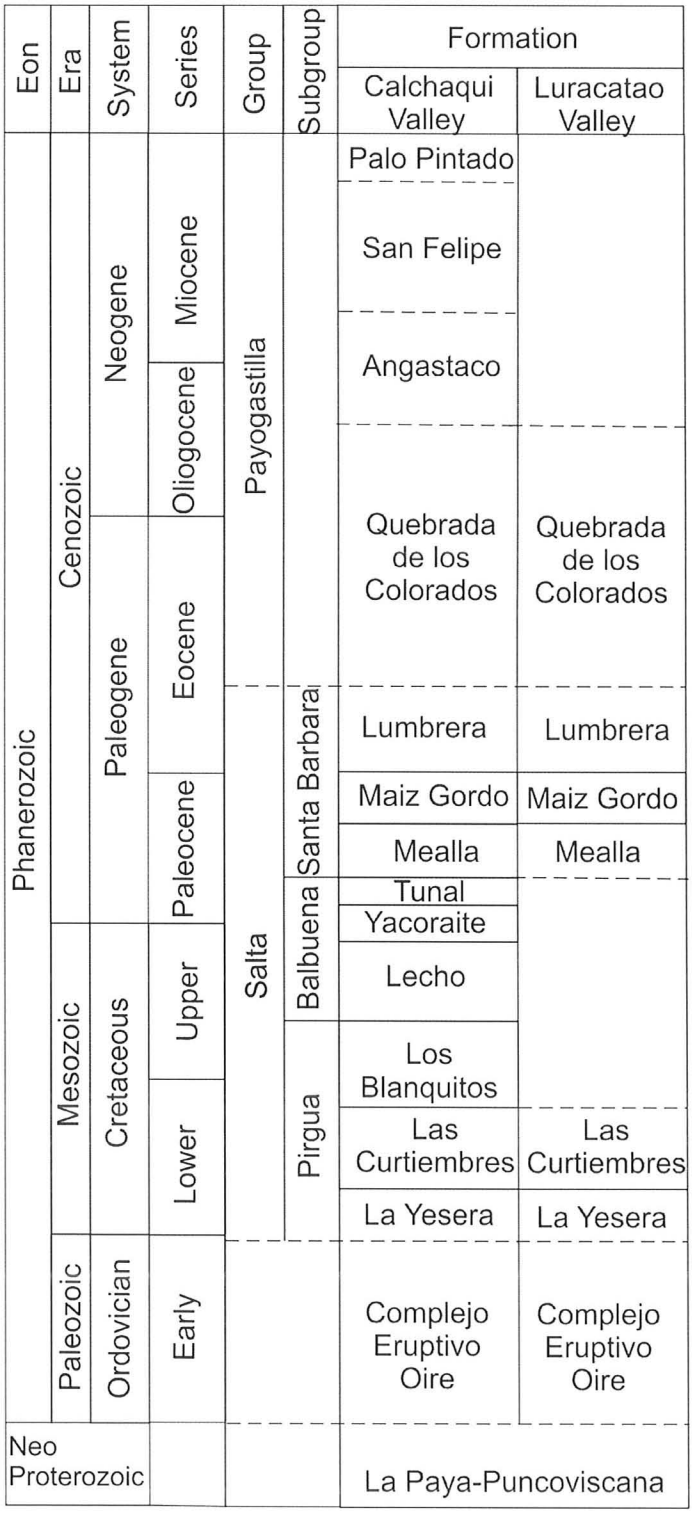

Figure 2- Stratigraphic section of the Calchaquí Valley and the Luracatao Valley (modified from Bosio et al., 2009).

Chapter 3: Structural characteristics of the Calchaquí Valley and Luracatao Valley

The Calchaquíes Valleys are located in the Eastern Cordillera and consist of the Calchaquí, Luracatao, Hualfin and Pucara Valleys (Fig. 1c). For this structural analysis, areas in the Calchaquí and southern Luracatao Valleys were investigated in detail. The Calchaquí Valley is bound by prominent first-order, N-S striking reverse faults, the Toro Muerto Fault and the Calchaquí Fault (Marrett et al., 1994). These faults juxtapose rocks of the Puncoviscana Formation (Mon and Salfity, 1995) over Cretaceous-Tertiary strata of the Salta Group (Moreno, 1970), which are exposed mostly in the center of the valley (Fig. 3). Quaternary alluvial deposits cover Paleozoic and Cenozoic rocks near the mountain fronts (Fig. 3). To the north, the Toro Muerto Fault and Calchaquí Fault terminate against the NW-SE striking, sinistral Olacapato-El Toro Fault Zone (Riller et al., 2001, Riller and Oncken, 2003; Petrinovic et al., 2005).

In the La Poma area, Cretaceous and Tertiary strata form a kilometre-scale, slightly asymmetric structural dome, known as the Cerro Bajo Dome (Hongn et al., 2007), that is cored by Puncoviscana Formation (Fig. 3, 4). To the north and south of this dome, the obliquity between NE-trending hinge lines of folded Tertiary strata and first-order reverse faults points to an overall sinistral transpressive deformation regime of the Calchaquí Valley during Tertiary times (Riller & Oncken, 2003).

The Luracatao Valley forms the westernmost valley of the Eastern Cordillera and is thus located close to the eastern margin of the Puna Plateau (Baldis et al., 1976; Salfity, 2008). The valley receives seasonal rain falls. Thus, the range bounding the valley to the west forms a local

orographic barrier to the adjacent Puna plateau. The structure of the Luracatao Valley is similar to that of the Calchaquí Valley. In particular, granitoid rocks of the Complejo Eruptivo Oire (Blasco and Zapettini, 1995) underlying the western valley flank are displaced over Tertiary rocks of the Eocene Quebrada de los Colorados Formation (Díaz et al., 1987) along the Refugio Fault (Fig. 1c). At the eastern valley flank, metasandstone of the Puncoviscana Formation and conglomerate of the Pirgua Formation are in contact with the Quebrada de los Colorados Formation at the Cachi Fault (Fig. 1c). The fault-fold geometry points to overall sinistral transpression in the Luracatao Valley during Tertiary times (Riller and Oncken, 2003; Bosio et al., 2009).

Chapter 4: Methods

In order to determine the process and style of deformation in the two valleys, characteristics of the first-order faults and its effects on the adjacent lithology was recorded through field mapping. The precise location of first-order reverse faults was mapped in the field. In some areas portions of the Puncoviscana Formation slumped over the exposed fault zone onto Tertiary strata. This potentially results in a false interpretation of the contact between these units as the fault plane. Therefore, only the damage zone between the Puncoviscana Formation and the Tertiary strata was recorded as the fault plane location. In addition, the orientations of higher-order fault planes, zones of cataclasite, foliation surfaces and aplitic dikes in granitoid rocks and bedding planes in Tertiary strata were measured. In the Quaternary deposits and Tertiary conglomerate, the shape-preferred orientation of fist-size boulders defined bedding planes. Fold-axial planes of folded bedding planes in these units were constructed from multiple bedding plane orientations. As maximum principal paleo-stress axes are assumed to be perpendicular to fold-axial planes, an approximate orientation of principal paleo-stress axis was inferred from the orientation of folds.

In inaccessible areas, the first-order reverse faults were traced on high resolution air photos and satellite images (Google Earth and Advanced Spaceborne Thermal Emission and Reflection (ASTER) satellite scenes with 90m resolution). The traces of reverse faults and a high-resolution digital elevation model (DEM) with 90m resolution were used to calculate the orientation of the fault plane at a given location using the three-point method. This method is based on the knowledge of the precise location of three points defining a plane, in this study the fault plane in X-Y-Z space. The calculated fault orientations were compared to field measurements of the

same fault to determine the validity of the method. For this analysis, application of the software *GeoTrig* by Rockware was particularly useful in areas where fault planes intersected canyons.

Acquisition of fault-slip data consisted of measuring the orientation of fault planes, the striations and the sense of movement on brittle shear faults at a given outcrop. In total 828 faults at 79 stations were measured. The quality of the slip-sense was recorded for better interpretation of the data. In areas where the sense of slip could not be identified reliably, e.g., close to the first-order reverse faults, a reverse sense of slip was given to the fault plane to comply with the faults with known sense-of-slip and the geological setting of the study area. In some cases, a normal sense of movement produced a more precise set of principal stress axes.

Analysis of the fault-slip data was performed using the software *Tectonics FP 1.6* (© Franz Reiter and Peter Acs). Processing a set of faults consisted of first checking the precision of the data using the *CHECK* algorithm. This algorithm ensures that for each fault plane in a set, the lineation recorded lies on the fault plane. Fault planes with lineations that deviate more than 10^{o} away from the fault plane were disregarded for further analysis. The corrected fault set was then used to calculate the orientation of the paleo-stress axes using one of three geometric methods that follow the Mohr-Coulomb criterion for brittle fracturing. The P-T-axes (Turner, 1953) method calculates the P-axis (shortening), T-axis (extension) and B-axis (orthogonal to both the P and T axes) for each fault plane and then produces a mean vector for these axes for the entire fault set. The direct inverse method calculates the stress tensor ($\sigma_1 > \sigma_2 > \sigma_3$) and stress ratio $R_{stress} = (\sigma_2-\sigma_3) / (\sigma_1-\sigma_3)$ (Angelier and Goguel, 1979; Sperner et al., 1993). The Numerical Dynamic Analysis (NDA) calculates the reciprocal strain tensor with axes $\lambda_1 > \lambda_2 > \lambda_3$ and strain

ratio $R_{strain} = (\lambda_2-\lambda_3) / (\lambda_1-\lambda_3)$ (Spang, 1972; Sperner and Ratchbacher, 1994). For all three analyses, the angle between the maximum principal stress axis and a given fault plane (θ) was assumed to be 30^{o}, which is a reasonable value according to the angle of internal friction (Byerlee, 1968; Sperner and Zweigel, 2010). For each fault set, the method used was based on the best fit of the principal axes to the fault set. To assess the quality of the result for each fault set, the number of faults with opposite sense of slip (negative expected value - *nev*) in the set was considered. In order to generate homogeneity of the fault sets, some sets had to be divided into homogeneous subsets. After comparison of the results from all methods, the NDA appears to be the best method for the majority of the fault sets in the study areas (Appendix A). Results from the P-T method are similar to those of the NDA and therefore, interpreted in terms of paleo-strain (Table 1, 2).

Field mapping, structural data and results of the fault-slip analysis were compiled and imported into *MapInfo Professional 10.0* (Pitney Bowes) to be displayed on geological maps. For a better understanding of the fault relationships, a 3D model of the first-order reverse fault planes in the Calchaquí Valley and the southern Luracatao Valley was constructed using the software *3D Geomodeller v.1.3.1* by Intrepid Geophysics. The orientation of the fault planes and structural data used for the model is based on the field data and calculated using the 3-point method. Fault planes were extrapolated to a depth of 3 km in the 3D models.

Table 1- Results of the fault-slip analysis for the Cerro Bajo Dome, Calchaquí Fault and Toro Muerto Fault in the La Poma area. n: number of brittle faults, P: shortening axis, T: intermediate axis , B: extension axis , nev: negative expected value (i.e. wrong shear sense)

Cerro Bajo Dome

		PTB			NDA					Inverse					
Station	n	P	T	B	σ1	σ2	σ3	Stress Ratio	nev	λ1	λ2	λ3	Stress Ratio	nev	Method Used
7-31	48	089/11	178/01	273/78	089/12	179/01	273/78	0.5598	5	079/17	170/03	268/73	0.5745	4	Inverse
6-196	23	106/09	015/01	276/81	107/08	017/01	280/82	0.5230	0	207/00	297/33	117/57	0.7641	2	NDA/PBT
6-219	22	111/16	020/00	288/74	112/13	022/02	283/77	0.5128	4	028/01	118/00	226/89	0.8422	4	NDA/PBT
6-203	17	116/13	026/03	284/77	115/13	025/02	288/77	0.5045	0	116/02	206/01	321/88	0.2246	0	NDA/PBT
6-194	17	078/49	340/03	249/57	061/37	158/10	260/52	0.6550	4	357/11	262/23	111/64	0.5019	9	NDA
6-225	16	085/02	174/11	032/82	105/02	195/04	345/85	0.6997	4	069/03	160/04	309/85	0.5862	5	NDA
6-191	14	105/10	015/04	265/80	105/10	015/03	266/79	0.5020	0	201/02	294/49	109/41	0.9859	5	NDA/PBT
7-210	20	238/01	329/04	063/83	Cannot be calculated					071/01	341/02	181/88	0.9394	0	PBT
6-197	6	328/08	149/18	291/75	068/30	183/37	310/39	0.6902	1	171/10	262/07	26/78	0.2255	1	NDA
6-201	5	080/32	183/17	300/42	071/44	199/32	309/28	0.8261	0	055/33	256/55	152/10	0.2646	1	PBT/NDA
6-202	5	108/01	018/03	213/88	108/01	018/02	215/87	0.5027	0	294/03	204/03	74/86	0.2321	0	NDA/PBT
6-212	4	266/02	175/04	021/85	267/02	177/06	018/84	0.4835	0	079/29	178/15	292/57	0.3279	2	NDA/PBT

Calchaquí Fault

		PTB			NDA					Inverse					
Station	n	P	T	B	σ1	σ2	σ3	Stress Ratio	nev	λ1	λ2	λ3	Stress Ratio	nev	Method Used
4-162	8	184/03	272/44	088/50	313/26	214/18	093/58	0.8932	1	191/03	037/86	281/02	0.5929	2	NDA
4-163	11	322/25	197/53	076/34	314/33	204/28	083/44	0.7680	2	353/31	183/59	085/05	0.5854	3	NDA/PBT
4-172	11	261/24	228/39	158/08	259/41	073/48	166/03	0.4796	1	134/62	300/27	033/06	0.5869	4	NDA/PBT
4-173	12	179/47	024/49	300/01	193/50	028/39	292/08	0.4253	2	181/28	031/59	278/13	0.3845	4	NDA
4-175	4	124/81	344/08	258/12	095/79	354/02	264/11	0.6906	0	244/29	114/48	350/26	0.5491	2	NDA/PBT
6-131	18	323/41	082/07	156/64	295/24	034/19	157/58	0.3418	6	241/82	086/07	356/03	0.893	9	NDA
6-123	12	273/04	176/07	029/83	121/11	031/01	293/79	0.4765	4	153/52	003/34	263/15	0.9447	4	PBT
6-121	5	147/05	242/43	042/43	144/07	242/44	047/45	0.4907	0	318/00	228/04	052/86	0.1966	0	NDA/PBT
6-126	4	296/30	165/35	048/36	306/19	198/43	053/41	0.4176	2	262/12	167/21	021/66	0.2874	2	NDA/PBT

Toro Muerto Fault

		PTB			NDA					Inverse					
Station	n	P	T	B	σ1	σ2	σ3	Stress Ratio	nev	λ1	λ2	λ3	Stress Ratio	nev	Method Used
7-132	14	256/34	151/27	065/40	257/37	163/07	064/52	0.4033	5	254/22	155/23	023/58	0.0476	7	PBT/NDA
4-1313	8	067/27	183/38	323/33	066/25	203/57	327/20	0.5962	1	091/22	182/04	280/67	0.2327	3	NDA
4-1314	10	289/06	180/42	002/57	110/06	205/38	012/51	0.6485	7	183/30	032/57	281/13	0.9654	1	PBT

Table 2- Results of the fault-slip analysis for the Refugio Fault in the Luracatao Valley. n: number of brittle faults, P: shortening axis, T: intermediate axis , B: extension axis , nev: negative expected value (i.e. wrong shear sense)

		PTB			NDA					Inverse					
Station	n	P	T	B	σ1	σ2	σ3	Stress Ratio	nev	λ1	λ2	λ3	Stress Ratio	nev	Method Used
7-251	22	289/39	127/40	249/69	294/26	120/64	025/03	0.1833	9	077/28	175/15	290/58	0.9409	7	NDA
4-281	6	073/30	169/03	244/64	064/26	332/03	237/64	0.7991	0	339/13	247/08	126/75	0.8362	0	NDA
4-282	9	059/09	151/13	279/78	065/09	155/04	271/80	0.4124	1	283/01	192/46	014/44	0.3762	3	NDA/PBT
4-285	5	170/43	297/15	043/34	159/21	267/40	048/43	0.3896	2	307/11	045/36	203/52	0.8469	2	NDA/PBT
4-289	5	016/27	296/28	110/47	358/31	245/33	120/41	0.5691	1	153/29	277/46	044/30	0.8711	2	PBT
4-2810	13	064/06	298/31	221/03	286/16	019/10	139/71	0.8189	3	031/02	300/10	132/80	0.7687	4	Inverse
4-2818	5	327/07	220/55	060/32	332/03	238/52	065/38	0.3657	2	324/08	216/64	058/24	0.0198	2	NDA
4-2819	8	130/10	185/41	280/60	141/10	232/11	014/75	0.0794	2	161/63	039/15	302/22	0.814	3	NDA
4-2820	14	256/02	334/37	164/52	261/08	354/21	151/67	0.1916	1	084/08	348/37	184/52	0.1662	5	PBT
4-2821	8	222/43	146/22	033/39	208/62	319/11	054/26	0.3357	3	027/76	166/10	257/09	0.8195	3	PBT
4-295	8	319/34	220/16	103/41	206/59	347/25	086/17	0.9344	1	160/04	252/21	058/69	0.8002	3	PBT
4-296	6	186/12	136/41	268/25	019/22	139/51	275/31	0.8626	2	067/84	178/02	269/06	0.6849	2	NDA
4-296 (b)	9	289/01	195/20	032/70	292/02	201/18	028/71	0.4066	0	098/02	188/16	359/74	0.2129	0	NDA
4-2913	7	083/72	314/46	201/19	333/53	163/37	069/05	0.4660	2	206/13	301/19	084/67	0.8632	3	NDA
4-2917	11	007/23	238/04	151/74	014/19	122/41	265/43	0.3508	2	184/15	276/08	033/73	0.5406	4	NDA
4-2918	5	313/23	213/34	075/57	312/20	214/20	083/62	0.6678	1	347/14	083/23	228/63	0.1787	2	NDA
4-2919	5	046/05	125/02	191/83	260/00	350/08	166/82	0.7165	1	187/28	296/31	063/46	0.4539	2	PBT
4-2920	6	090/16	218/70	003/29	106/19	216/45	359/38	0.4164	2	079/10	331/61	174/27	0.2378	3	NDA
4-308	7	060/15	331/31	153/67	054/14	312/18	191/71	0.5209	1	208/13	300/09	063/74	0.3791	1	PBT/NDA
4-3015	14	026/24	267/22	153/35	035/23	290/30	156/50	0.4028	6	233/01	142/22	325/68	0.6846	4	PBT
4-3019	18	316/02	176/49	032/30	133/07	233/56	039/33	0.2681	3	343/05	251/22	086/68	0.5608	6	NDA
5-11	6	186/47	314/37	069/17	213/75	001/13	092/08	0.7075	1	184/53	347/36	083/08	0.1466	1	NDA
5-13	5	283/06	179/66	016/24	283/05	181/62	016/26	0.5187	0	196/63	335/19	070/14	0.9374	1	NDA
5-13 (b)	7	019/02	340/46	108/10	019/14	115/22	259/63	0.3478	0	032/08	294/45	129/44	0.426	2	NDA
5-14	12	224/22	294/05	351/82	262/05	170/24	003/65	0.5210	2	178/12	081/28	288/59	0.1207	4	NDA
5-15	15	319/22	042/28	171/46	108/04	016/28	206/62	0.6269	4	334/07	065/10	209/78	0.4643	6	NDA
5-111	6	084/13	342/49	186/39	083/14	337/50	184/37	0.4115	0	227/17	325/25	106/59	0.4612	2	PBT/NDA
5-114	7	154/09	292/67	197/24	329/04	062/45	235/45	0.4698	3	078/35	279/53	175/10	0.7984	2	NDA
5-22	8	057/05	327/29	166/80	054/06	145/05	277/82	0.7502	1	105/00	195/71	014/19	0.684	3	NDA
5-210	6	280/15	187/21	063/61	269/21	177/07	069/68	0.5259	0	285/23	038/43	176/38	0.4259	0	PBT

Table 3- Results of the fault-slip analysis for the Cachi Fault and Luracatao Fault in the Luracatao Valley. n: number of brittle faults, P: shortening axis, T: intermediate axis , B: extension axis , nev: negative expected value (i.e. wrong shear sense)

Cachi Fault

		PTB			NDA					Inverse					
Station	n	P	T	B	σ1	σ2	σ3	Stress Ratio	nev	λ1	λ2	λ3	Stress Ratio	nev	Method Used
7-181	7	200/61	160/06	342/66	200/40	090/22	338/42	0.6499	1	053/11	322/03	218/78	0.9003	0	Inverse
3-141	23	242/34	040/37	134/35	214/14	323/52	114/34	0.6317	9	193/09	97/33	297/56	0.5071	5	NDA
3-163	16	256/22	157/23	125/75	286/38	020/04	115/52	0.6635	7	033/73	267/10	174/14	0.9597	8	PBT
3-168	15	263/31	165/16	052/54	251/32	156/08	054/56	0.6751	3	075/09	167/13	312/74	0.747	4	NDA/PBT
5-32	19	258/26	000/19	129/60	261/29	002/19	121/54	0.7851	4	009/16	100/03	201/74	0.3946	5	NDA/PBT
5-35	12	281/02	142/48	011/43	109/08	200/05	324/81	0.5304	2	181/03	271/02	039/86	0.2545	2	PBT
5-36	7	330/18	116/71	232/10	335/65	137/24	230/07	0.7987	1	342/41	208/39	096/25	0.3473	2	NDA
5-37	14	267/06	357/32	167/60	272/07	005/24	167/65	0.4798	2	003/14	270/08	152/73	0.3809	2	NDA/PBT
5-38	13	241/43	081/54	340/01	293/50	068/31	173/23	0.3271	6	351/08	087/39	252/50	0.9434	5	NDA
5-39	25	113/01	007/52	211/33	304/04	038/43	210/47	0.3272	10	095/01	002/64	185/26	0.1996	9	PBT
5-41	4	293/32	209/01	119/55	288/27	019/01	111/63	0.4394	1	285/44	167/26	058/34	0.0798	2	NDA/PBT
5-42	6	302/09	107/34	234/55	343/12	077/19	222/67	0.6272	1	091/06	269/84	001/00	0.7269	3	PBT
5-46	11	250/38	071/65	356/07	256/47	097/41	357/10	0.3845	3	190/31	035/56	288/11	0.5574	4	NDA/PBT

Luracatao Fault

		PTB			NDA					Inverse					
Station	n	P	T	B	σ1	σ2	σ3	Stress Ratio	nev	λ1	λ2	λ3	Stress Ratio	nev	Method Used
3-152	13	110/19	360/10	283/52	102/23	199/15	319/62	0.5827	3	008/00	277/18	099/72	0.7254	5	NDA/PBT
3-154	5	006/08	189/56	081/01	003/05	270/31	102/59	0.2636	1	233/02	140/54	325/36	0.7904	2	NDA/PBT

Chapter 5: Structure of the La Poma area

The Toro Muerto Fault, the Calchaquí Fault and the Cerro Bajo Dome form the most conspicuous structures in the La Poma area (Fig. 3). The areal extent (circumference) of the Dome is well defined by the concentric strike of inclined strata of the Lecho, Yacoraite, Mealla and Quebrada de los Colorados Formations (Fig. 4). The Dome is asymmetric in plan view and profile plane (Fig. 3, 4). Specifically, it is elongated in the N-S direction and characterized by a curved hinge zone trace (Fig. 3). Moreover, sedimentary strata defining the east limb of the Dome dip moderately eastward and display decameter-scale, asymmetric folds with east-dipping fold-axial planes (Fig. 4). The western portion of the Dome is mostly obscured by rocks of the Puncoviscana Formation that were thrust over Cretaceous and Tertiary strata of the Dome on the Toro Muerto Fault (Fig. 4).

The southwestern portion of the Cerro Bajo Dome is cut by the Cerro Bajo Fault, a steeply east-dipping reverse fault that juxtaposes the Yacoraite and underlying Lecho Formations in the hanging wall against steeply west-dipping Tertiary strata in the footwall (Fig. 5a). The Cerro Bajo Fault is believed to be a splay of the Calchaquí Fault (Hongn et al., 2007) and is cut by the Toro Muerto Fault (Fig. 3). North of the Cerro Bajo Dome, strata of the Eocene Quebrada de los Colorados Formation form a prominent anticline with a N-S trending hinge zone (Fig. 3). Strata of the east limb of the Dome shallow with distance from its hinge zone and are locally overturned in the footwall of the Calchaquí Fault (Fig. 5b). The Calchaquí Fault branches into two fault splays, one of which is spatially associated with the Quaternary basaltic to andesitic Gemelos volcanoes (Guzmán et al., 2006). Alluvial and lacustrine Quaternary deposits cover the

deformed Cretaceous and Tertiary strata and are displaced by reverse faults such as the so-called Barbaro Fault near the Calchaquí River (Fig. 5c).

In order to understand better the kinematics and displacement magnitude of first-order faults, notably of the Toro Muerto Fault, the precise orientation of this fault must be known. This was accomplished by recording the fault orientation in the field where outcrop permitted such measurements (Fig. 5d) and by tracing the exposed fault plane on stereo photos (Fig. 3). In combination with digital elevation models derived from ASTER satellite scenes, fault orientations were obtained by interpolating the positions of three locations of fault exposures on a given fault segment in X-Y-Z space using the software *GeoTrig* (Rockware). Information on the orientation of individual fault segments was then used to model the fault surface in three dimensions (Fig. 6) using the software *Geomodeller* (Intrepid Geophysics).

Overall, the Toro Muerto Fault dips shallowly (10^{o}-15^{o}) to the west. However, some fault segments of this fault dip shallowly to the east. The modelled orientation and curvi-linear trace of the Toro Muerto Fault suggests that the fault surface undulates about hinge lines dipping shallowly toward the SW. This may either be a primary characteristic of the fault or caused by open folding of the surface (Fig. 3). The Calchaquí Fault dips steeper (25^{o}-35^{o}) than the Toro Muerto Fault. However, unlike the Toro Muerto Fault the splay of the Calchaquí Fault west of the Gemelos volcanoes is rather straight in map view and, thus, must dip rather steeply (Fig. 3).

Hand-drawn trajectories of inclined bedding planes in the folded Tertiary strata can be used to estimate the circumference of the Cerro Bajo Dome and, thus, the displacement magnitude on the

Toro Muerto Fault. This estimate is based on the width of the Dome portion that is overridden by the Puncoviscana Formation on the Toro Muerto Fault. The width of the overridden Dome portion is interpolated using the trajectory shapes from exposed bedding planes east of the fault (Fig. 3). Assuming an average dip of 20° for the Toro Muerto Fault, the estimated displacement magnitude on the fault surface amounts to a minimum of 2480 m (Fig. 3).

In summary, two major deformation increments are evident from the La Poma area. The first increment is characterized by the formation of the Cerro Bajo Dome and displacement on the Cerro Bajo Reverse Fault. This increment must have occurred after the Eocene as it affected the Quebrada de los Colorados Formation. Displacement of the Puncoviscana Formation over the western Cerro Bajo Dome and truncation of the Cerro Bajo Fault by the Toro Muerto Fault characterizes the second deformation increment. Thrusting on the Toro Muerto Fault and reverse faulting on the Calchaquí Fault are key elements of this deformation. The two deformation increments differ in style, i.e. non-cylindrical deformation in the first and cylindrical deformation in the second increment. Deformation continued to Quaternary times as indicated by displacement of Quaternary strata on the Barbaro Fault (Fig. 5c).

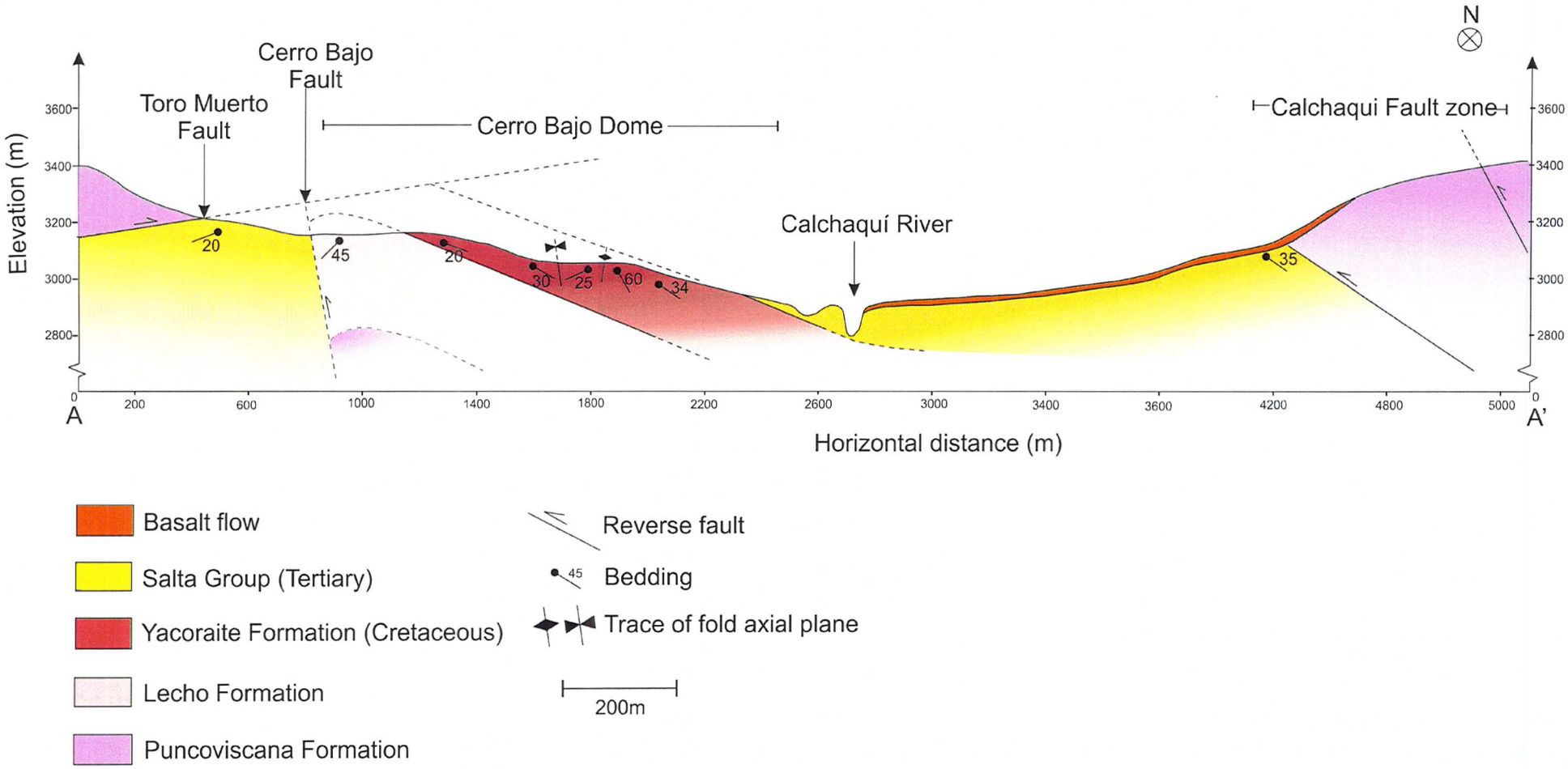

Figure 4- Cross-section A-A' showing the structure of the Cerro Bajo Dome.

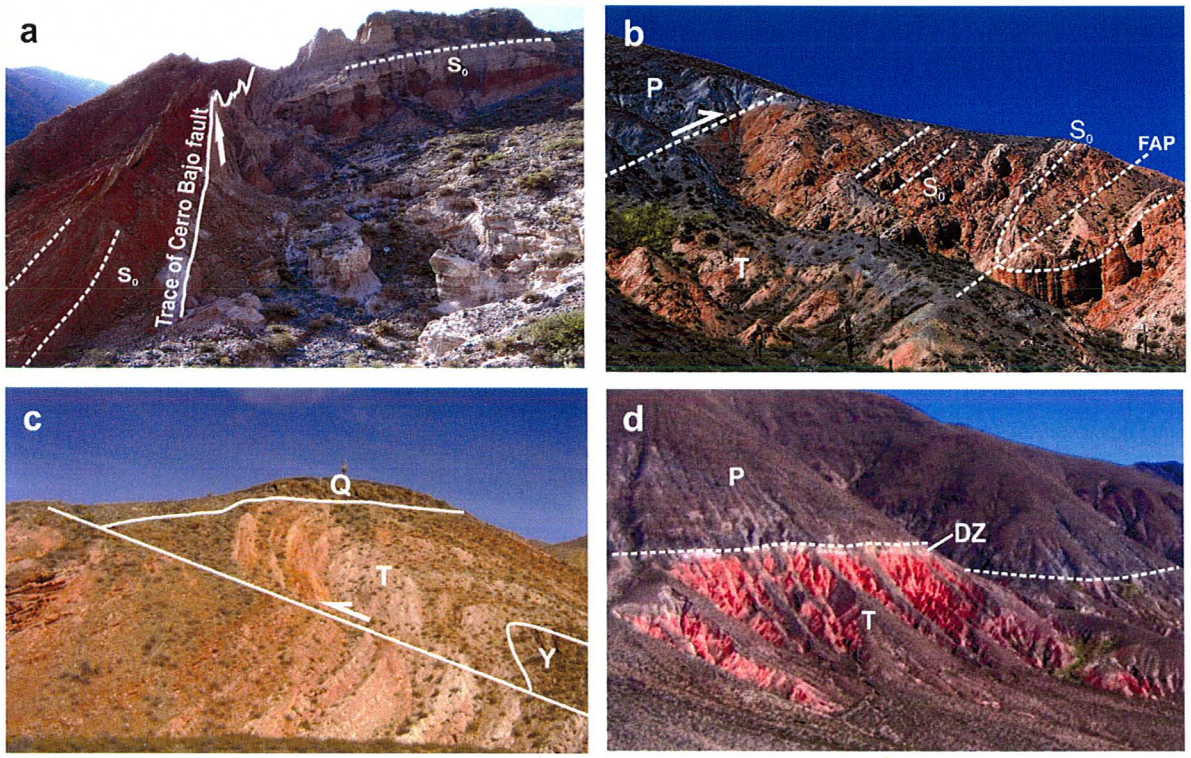

Figure 5- Colour plate showing structural field characteristics of the La Poma area. S_o delineates bedding planes. (a) Trace of the Cerro Bajo Fault. (b) Trace of the Calchaquí Fault juxtaposing Puncoviscana Formation (P) against Tertiary rocks (T). Deformation also includes folding of the Tertiary strata due to faulting. FAP delineates the fold axial plane of the recumbent fold. (c) The Barbaro Fault Zone displacing Quaternary strata (Q) overlying the Tertiary (T) rocks and Yacoraite Formation (Y). (d) Trace of the Toro Muerto Fault displacing Puncoviscana Formation (P) over Tertiary rocks (T). DZ delineates the damage zone of the Toro Muerto Fault.

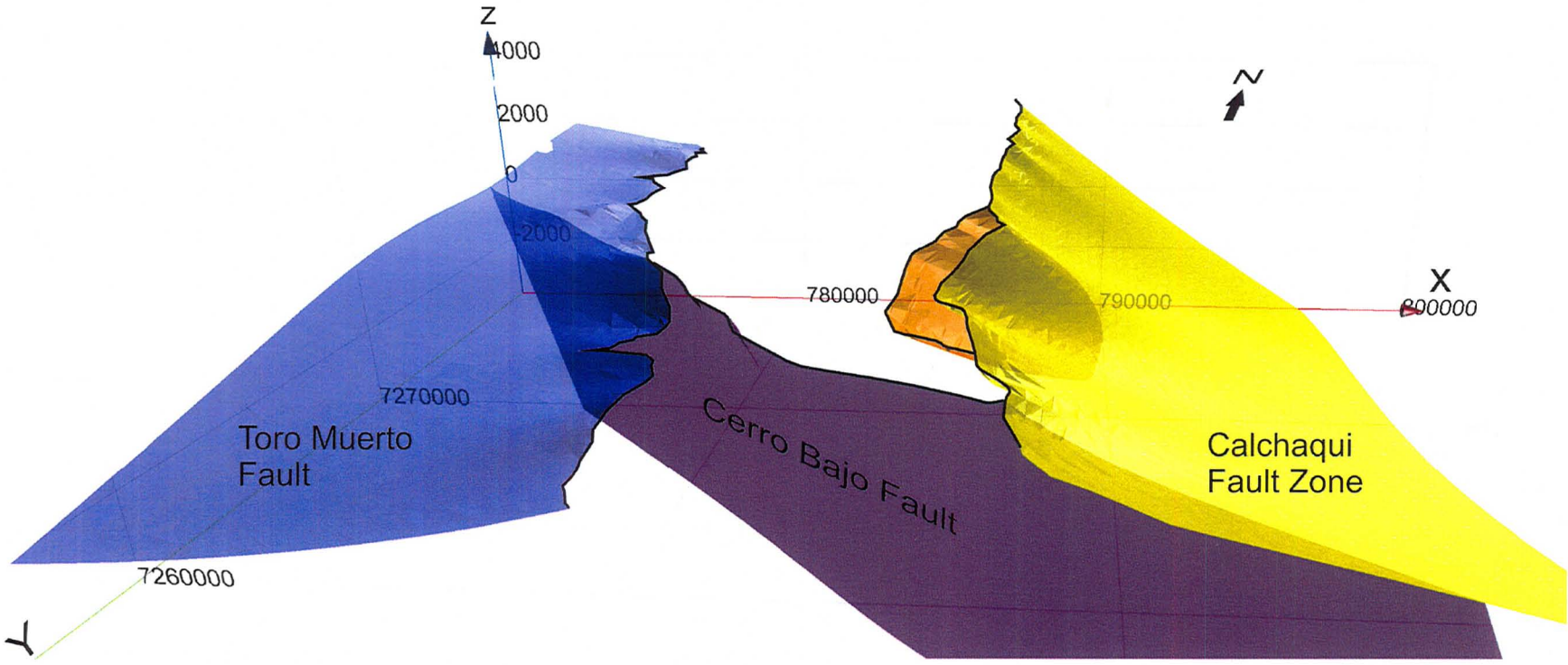

Figure 6- 3D model of the Toro Muerto Fault, Calchaquí Fault Zone and the Cerro Bajo Fault in the La Poma area.

Chapter 6: Structure of the southern Luracatao Valley

The southern Luracatao Valley trends NNW-SSE and lies on the westernmost edge of the Eastern Cordillera, where the western range of the valley is an orographic barrier to the Puna Plateau. Like the Calchaquí Valley, the Luracatao Valley is also lined with approximately N-S striking reverse faults of opposite dip direction. The east range of the valley is lined by the Cachi Fault and the west range is lined by the Luracatao Fault and Refugio Fault (Fig. 7). On the scale of the entire Luracatao Valley, the trace of the Cachi fault trends N-S. However in the southern part of the valley the fault curves to the SE (Fig. 7). The center of the valley consists of folded Tertiary strata of the Quebrada de los Colorados Formation covered in most areas by Quaternary deposits (Bosio et al., 2009).

The Cachi Fault juxtapositions conglomerate of the Cretaceous Pirgua subgroup against Quaternary strata that are unconformably lying over the Tertiary strata of the Quebrada de los Colorados Formation (Fig. 8a, b). The Cachi Fault has an average dip of 60°, and was a Cretaceous growth fault that has been reactivated as a reverse fault (Fig. 8c; Riller and Hongn, 2003). Proximal to the fault, Tertiary strata are overturned and Quaternary deposits, cemented by the precipitation of carbonate minerals, are buckled due to the top to west movement of the Pirgua conglomerate on the Cachi Fault (Fig. 8a). East of the Cachi Fault, a km-scale syncline in the Pirgua Formation, known as the Brealito Syncline, is evident (Fig. 7). The fold axis of this syncline curves southward into the fault plane of the Cachi Fault suggesting that the fault is younger than the syncline and a has a sinistral sense of movement (Riller and Hongn, 2003).

On the west range of the valley, granite of the Ordovician Oire Complex is displaced over sedimentary rocks of Tertiary Quebrada de los Colorados Formation (Blasco and Zapettini, 1995) on the Luracatao Fault and Refugio Fault (Fig. 7, 9). The Luracatao Fault appears to be transected by the Refugio Fault (Hongn and Seggiaro, 2001). The two faults dip at angles of approximately 40°. However, 3D modeling based on orientations of the fault plane segments inferred from field mapping shows a shallowing of the Luracatao Fault towards the intersection with the Refugio Fault (Fig. 10).

Interestingly, the Refugio Fault is concordant to the metamorphic foliation in metagranite and felsic dykes in the hanging wall of the faults (Fig. 7, 8d). Thus, the orientation of the fault planes may be controlled by the structural anisotropy imparted by previous ductile deformation in the granitoid Oire complex (see also Hongn and Seggiaro, 2001; Riller and Hongn, 2003). The Luracatao Fault in relation to the Refugio Fault is shallower as seen in the 3D model. Thus, the presence of the Refugio Fault and the curving trace of the Luracatao Fault affect the dip of the fault plane. The presense of 20 – 50 cm wide cataclastic deformation zones is of considerable interest in this area. These zones are replete with angular host rock fragments in a matrix of aqueous minerals indicating the influence of fluids (most likely surface precipitation) on the mechanics of the faulting (Fig. 8e, f). The influence of aqueous fluids at this orographic barrier can affect the deformation process on the meter as well as on the millimeter scales.

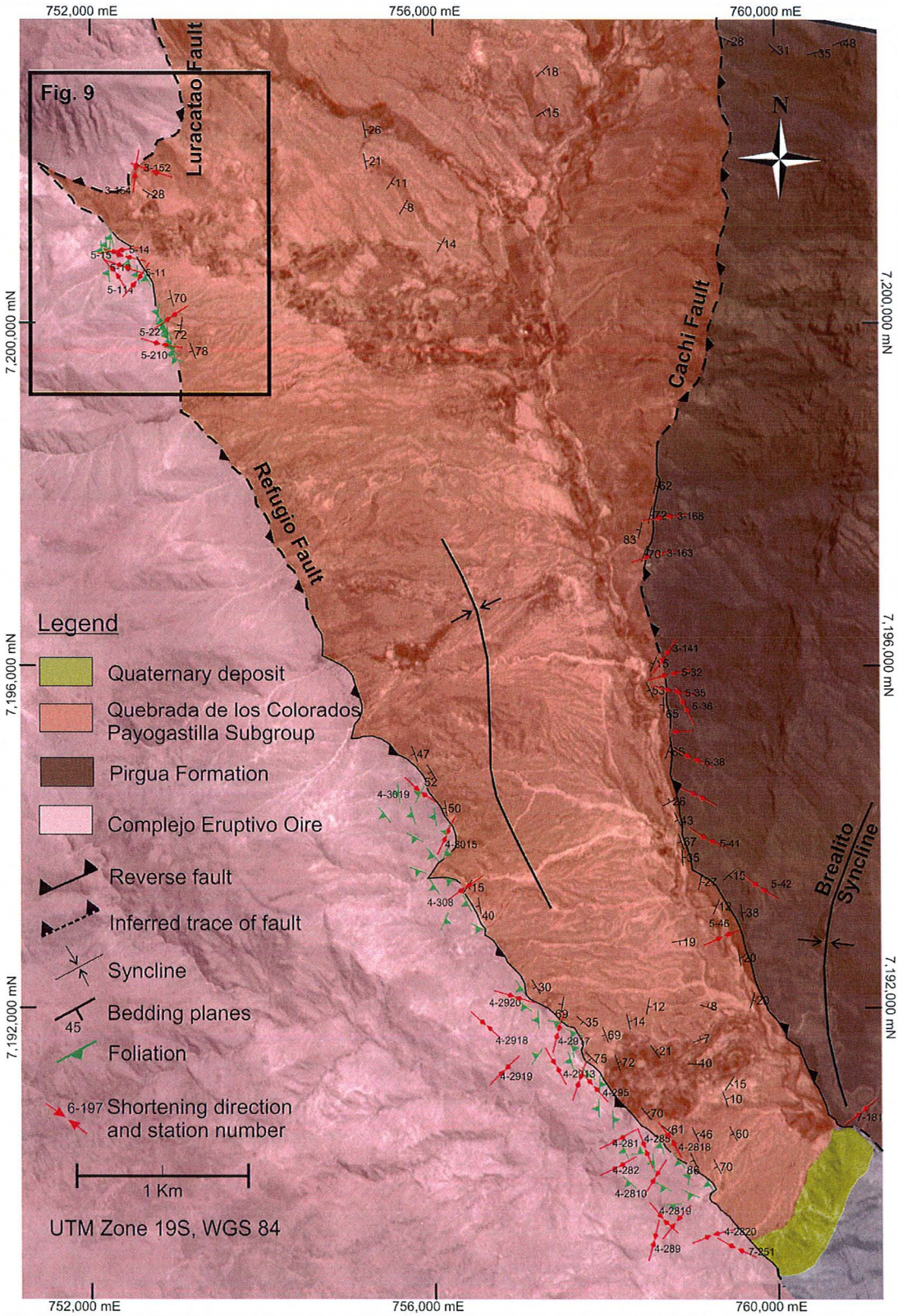

Figure 7- Geological units and structure of the Luracatao Valley draped over an airphoto.

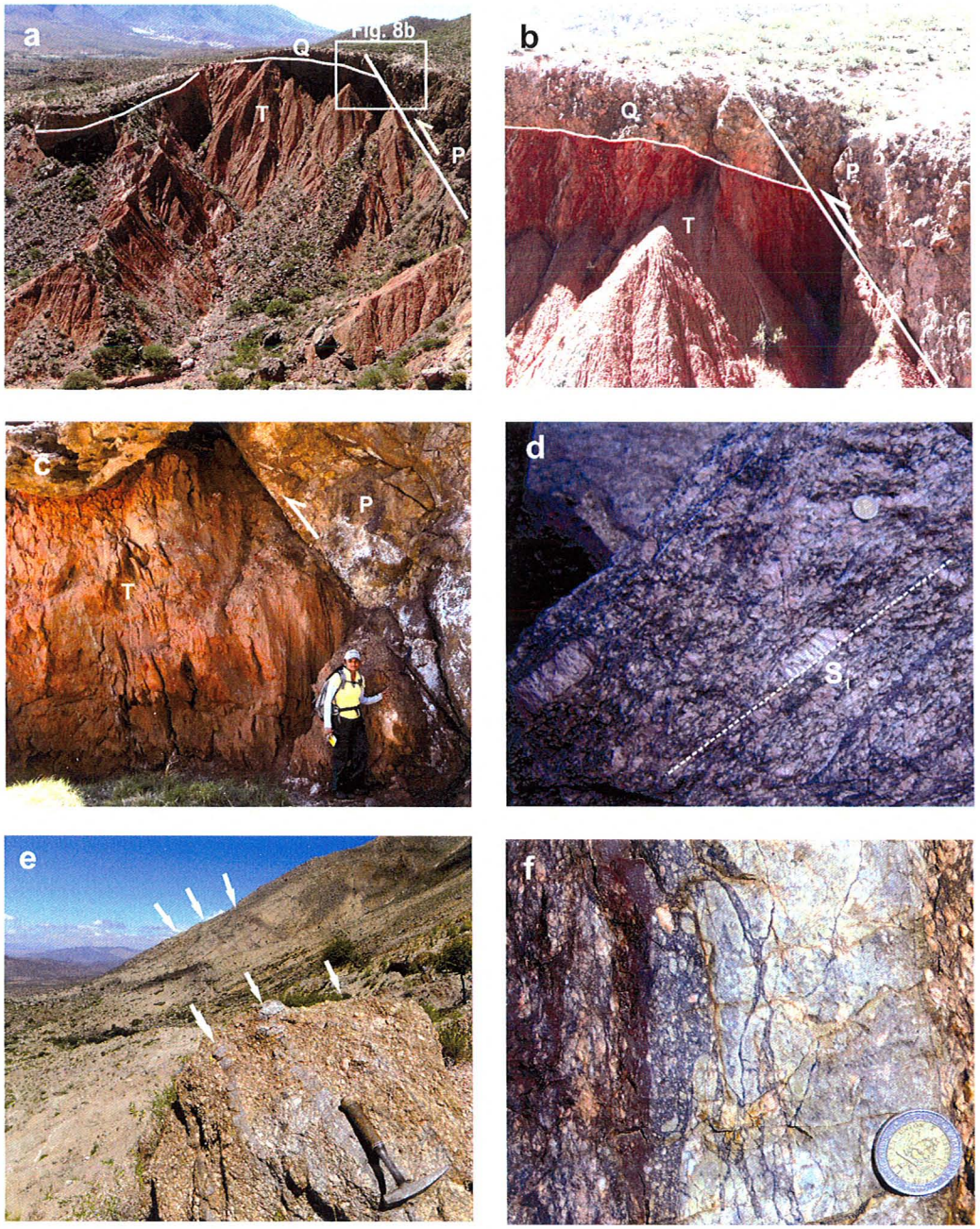

Figure 8- Colour plate showing structural field characteristics of the Luracatao Valley. (a) Quaternary (Q) deformation on the Cachi Fault. Note the buckling of the Quaternary strata due to the top movement of the fault. (b) Close-up of Pirgua Formation (P) juxtaposed against Quaternary rock (Q) at the Cachi Fault. (c) Fault plane of the Cachi Fault juxtaposing Pirgua Formation (P) against Tertiary rock (T). (d) Foliation (S_1) in the metagranitiod rock of the Complejo Eruptivo Oire near the Refugio Fault. (e) Cataclasite zones in the Complejo Eruptivo Oire near the intersection of the Luracatao Fault and Refugio Fault. (f) Close-up of the cataclasite zones in the metagranitoid rocks.

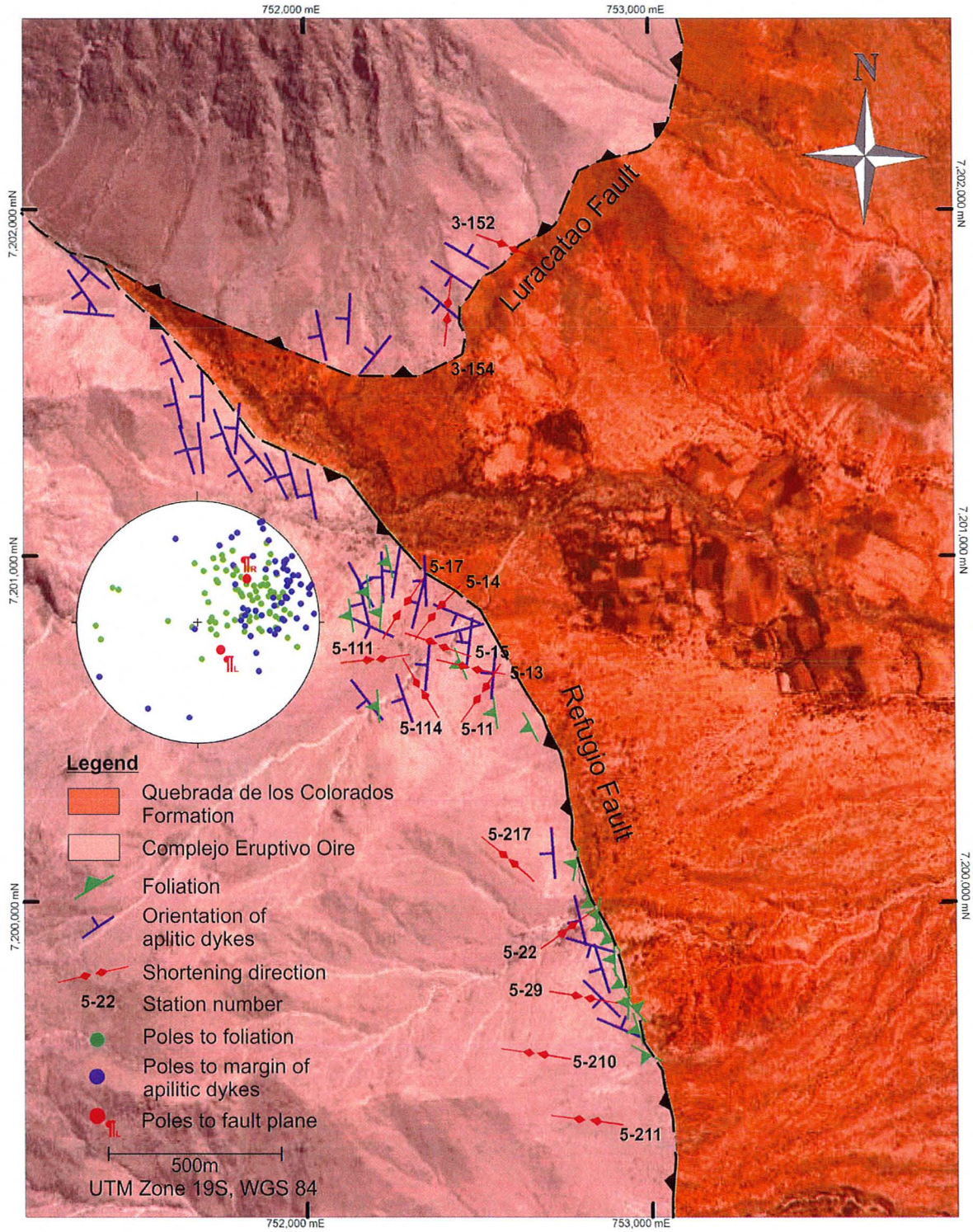

Figure 9- Geological map showing the intersection of the Luracatao Fault and the Refugio Fault. Lower-hemisphere, equal-area projection shows poles to foliation planes (green), poles to margin of aplitic dykes (blue) and pole to fault planes (red) in meta-granitoid rocks of the Complejo Oire.

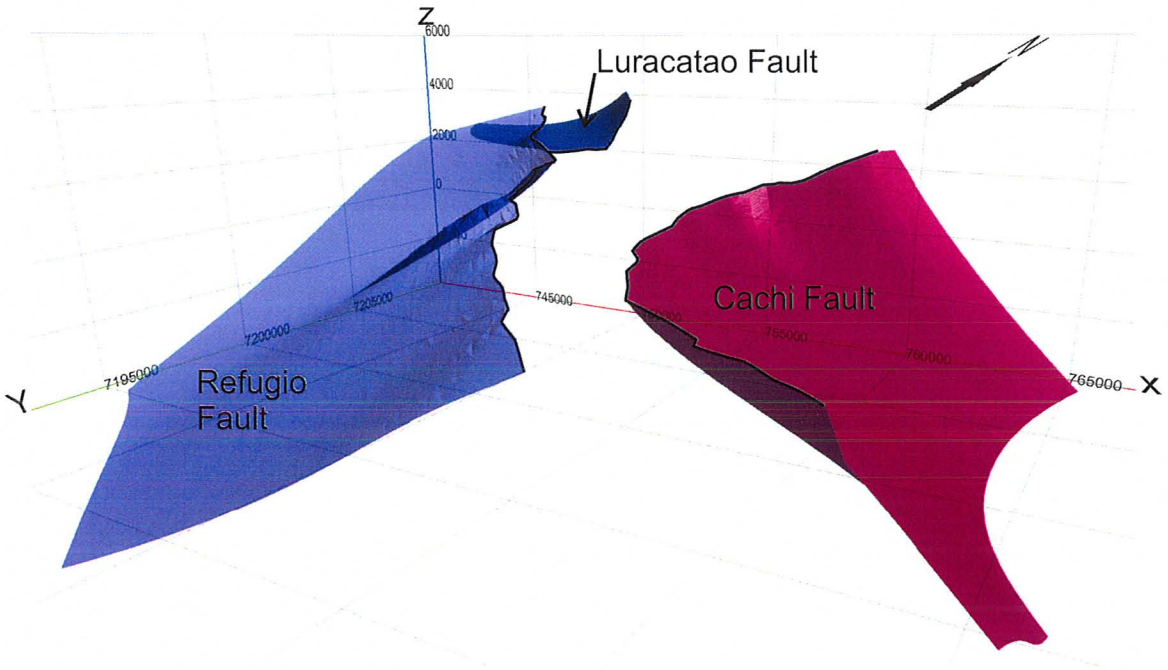

Figure 10- 3D model showing the Refugio Fault, the Luracatao Fault and the Cachi Fault in the Luracatao Valley.

Chapter 7: Structure of the Cachi area

The Cachi study area is situated in the center and widest part of the Calchaquí Valley (Fig. 1c). Here the exposed lithologies consist of coarse Quaternary conglomerate overlying Tertiary sandstone. The Quaternary deposits can be subdivided into two units, Unit 1 and Unit 2 (Fig. 11). Unit 1 covers unconformably tilted strata of, and is thus younger than, Unit 2 (Fig. 12a). Unit 2 has a yellowish matrix containing poorly sorted clasts of several crystalline rock types. These include granitoid rocks, cordierite schist, meta-granodiorite, biotite gneiss, chloritized granite and foliated metagranite that are typical for the Cachi Range west of the study area (Turner, 1960). By contrast, Unit 1 consists chiefly of clasts of the Puncoviscana Formation set in a red matrix and is derived from the eastern valley flank. Therefore, uplift of the Cachi Range preceded that of the eastern valley flank. This change in exhumation was accompanied by a westward shift of the Calchaquí River to its present position at the mountain front of the Cachi Range. Collectively, this attests to active landscape evolution of the Valle Calchaquí during the Quaternary.

Deformation of Quaternary deposits is evident from the variation in bedding plane orientations, defined by the shape-preferred orientation of elongate clasts. The curvature of the Quaternary bedding planes and contacts of the Quaternary lithological units in map view points to the presence of a kilometer-scale cylindrical anticline. The anticline is cored by Tertiary strata and is characterized by a NNE-SSW trending axis (projection in Fig. 11) and a steeply SE-dipping fold axial plane (projection in Fig. 11, 12d). In the west limb of the anticline, bedding planes of Unit 2 steepen toward the fold axis. Here, the geometry of meter-scale folds along with the variation

in bedding planes suggests top-to-NW displacement (Fig. 12b, c). The structural relationships suggest that Unit 1 forms the hanging wall of a prominent east-dipping reverse fault near overturned strata of Unit 2 (Fig. 11). The orientation of the fault plane is assumed to be concordant to the NNE-SSW trending fold-axial plane (projection in Fig. 11) and thus indicates NW-SE shortening during Quaternary times.

The Cachi area hosts also a large structural dome, the Cerro Tintin Dome (Fig. 1b), located immediately east of the Quaternary anticline (Fig. 1c). The Dome consists of Cretaceous and Tertiary strata and is cored by the Puncoviscana Formation. In the Cachi area, the Quaternary anticline, the Quaternary bedding planes are shallower than the underlying Tertiary strata. Thus, cylindrical folding and associated reverse faulting commenced in the Tertiary and continued to be active in the Quaternary. This suggests that deposition of Quaternary units occurred during folding. In summary, first-order structural characteristics of the Cachi area are similar to those of the La Poma area, i.e., doming was followed by orogen-parallel cylindrical folding and reverse faulting.

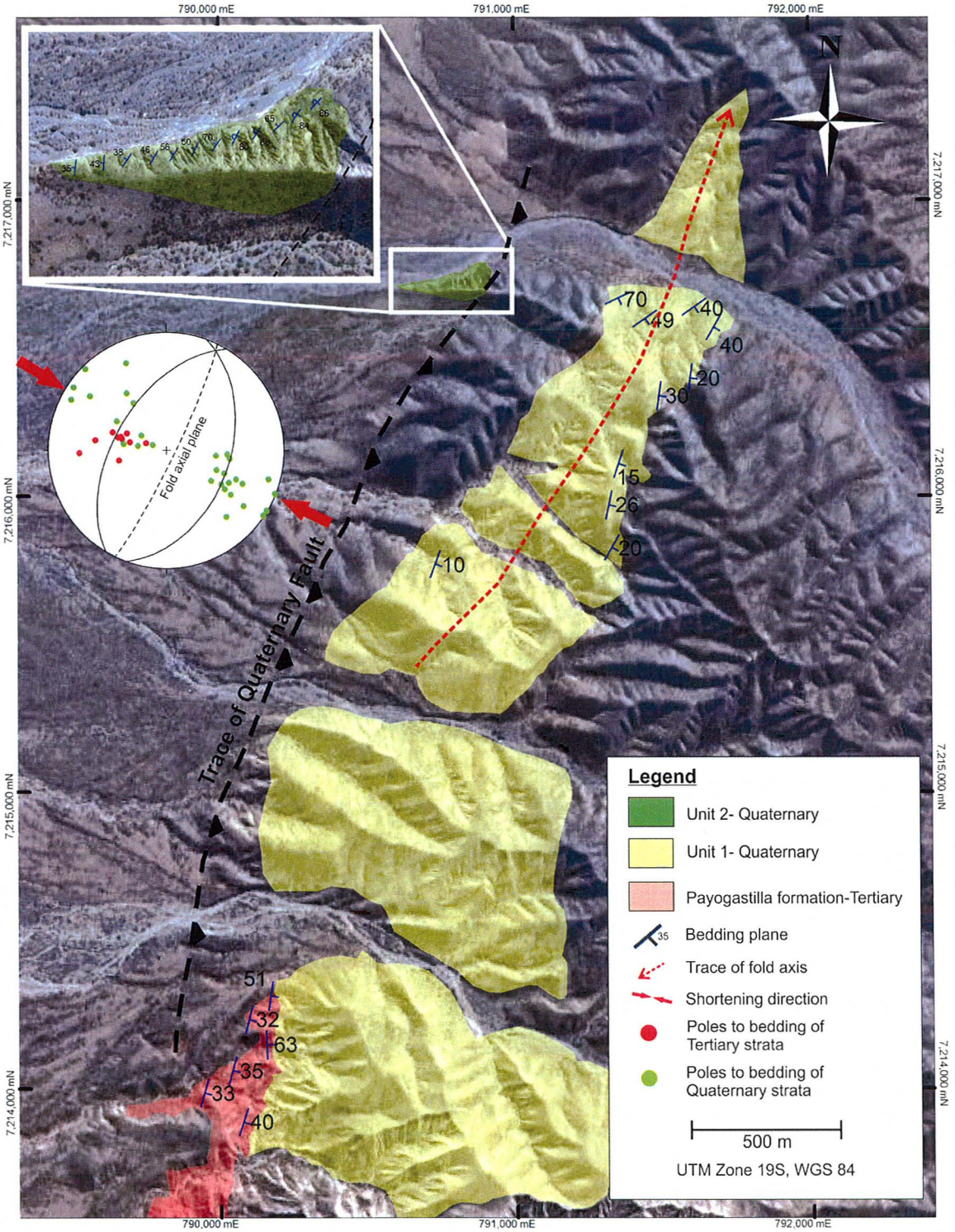

Figure 11- Geological units and structure of the Cachi area draped over Google Earth image. Lower-hemisphere equal-area projection shows poles to bedding of Quaternary (green) and Tertiary strata (red), the constructed fold axial plane and the inferred principal paleo-stress axes perpendicular to the fold axial plane.

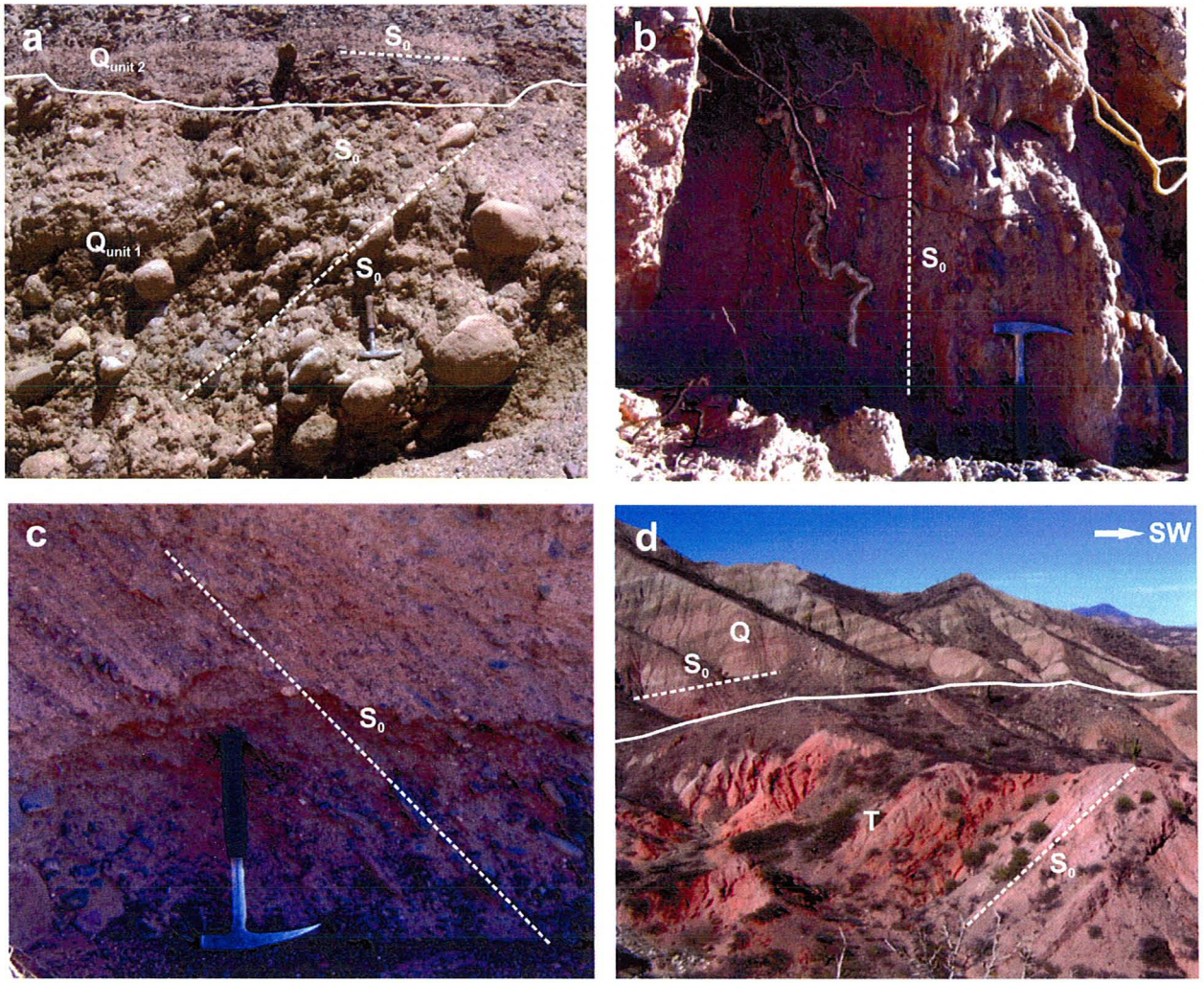

Figure 12- Colour plate showing structural field characteristics of the Cachi area. S_0 delineates trace of the bedding plane. (a) Variation in the steepness of bedding planes between Unit 1 and Unit 2 of the Quaternary deposits. (b) Steepness of the bedding planes visible from the alignment of the boulders in the Unit 1 Quaternary deposit. (c) Aligned clasts from the Puncoviscana Formation in the Unit 1 Quaternary deposit. (d) Relationship between the orientations of bedding planes in the Quaternary deposit (Q) and the Tertiary units (T).

Chapter 8: Fault-Slip Analysis

Directions of shortening and extension were inferred from small-scale brittle shear faults near first-order structures in the Calchaquí Valley and Luracatao Valley to better understand the kinematics of prominent late Tertiary structures. In the La Poma area, the kinematics of brittle faults was recorded in rocks of the Puncoviscana Formation that were affected by the Toro Muerto Fault and Calchaquí Fault and of the Yacoraite Formation that shaped the Cerro Bajo Dome. In the Luracatao Valley, fault-slip data was recorded in the Cretaceous Pirgua Formation that was deformed by the Cachi Fault and in granitoid rocks of the Ordovician Oire Complex at the Refugio Fault.

8.1 La Poma

Brittle faults on the Calchaquí Fault have a variety of orientations with dominantly NW and SE plunging striations (Fig. 13b). The Toro Muerto fault has dominantly SW dipping brittle faults with W-plunging striations. On the Cerro Bajo Dome brittle faults dip mostly to the east which is concordant to the bedding planes in the Yacoraite Formation (Fig. 13c). Here, the striations are E-plunging. Fault-slip analysis on the Cerro Bajo Dome reveals a difference in the style of deformation between the Yacoraite Formation and the Mealla Formation. This is evident in particular by the orientation of striations on a given fault plane of a conjugate set in the Yacoraite Formation and the orientation of faults and respective striations in the Mealla Formation. Striations on brittle faults in the Yacoraite Formation display uniform orientations, whereas individual brittle faults in the Mealla Formation often show multiple orientations of striations (e.g., Station 7-210 in Appendix A). This difference in the style of brittle faulting between the

two lithologies may be due to the different structural anisotropies between the strongly layered carbonate beds of the Yacoraite and structurally less anisotropic conglomerate and sandstone units of the Mealla Formation. The variable orientation of the striae on a single fault plane in the sandstone may also indicate changes in shortening direction during progressive deformation. In particular, the two lithologies show different deformational behavior under the same deformation regime making the sandstone more susceptible to deformation.

Brittle faults associated with the Cerro Bajo Dome and the Toro Muerto Fault indicate subhorizontal E-W shortening and subvertical extension (Fig. 13a, c). In contrast, brittle faults associated with the Calchaqui Fault indicate mostly NW-SE shortening (Fig. 13b). The obliquity between shortening direction and strike of the Calchaquí Fault points to a left-lateral component of displacement on this fault.

8.2 Luracatao Valley

The brittle faults and striations associated with the Refugio Fault in the Luracatao Valley have a variety of orientations (Fig. 13d). The brittle faults of the Cachi fault also show a variety of orientations but with dominantly east and west plunging striations (Appendix A). Thus, shortening direction of the first-order reverse faults on either side of the valley have varying orientations. The orientations of brittle fault planes along the Refugio Fault are highly variable and respective striations are poorly preserved making it difficult to determine the sense of movement on a given fault. Therefore, the precision of the shortening direction is compromised. In this data set of the Refugio Fault, it is also evident that movement and thus striations often formed along pre-existing fault planes. Thus, the variation in shortening directions may also

depend on the orientation of the brittle fault planes and pre-existing structural anisotropy of the granitoid rocks. Shortening is subhorizontal with subvertical extension on the Refugio Fault (Fig 13d). In contrast, shortening associated with the Cachi Fault is mostly E-W and NW-SE (Fig. 13e). Thus, shortening directions are oblique to the Cachi Fault and indicate an overall left-lateral sense of movement on this fault (Fig. 13).

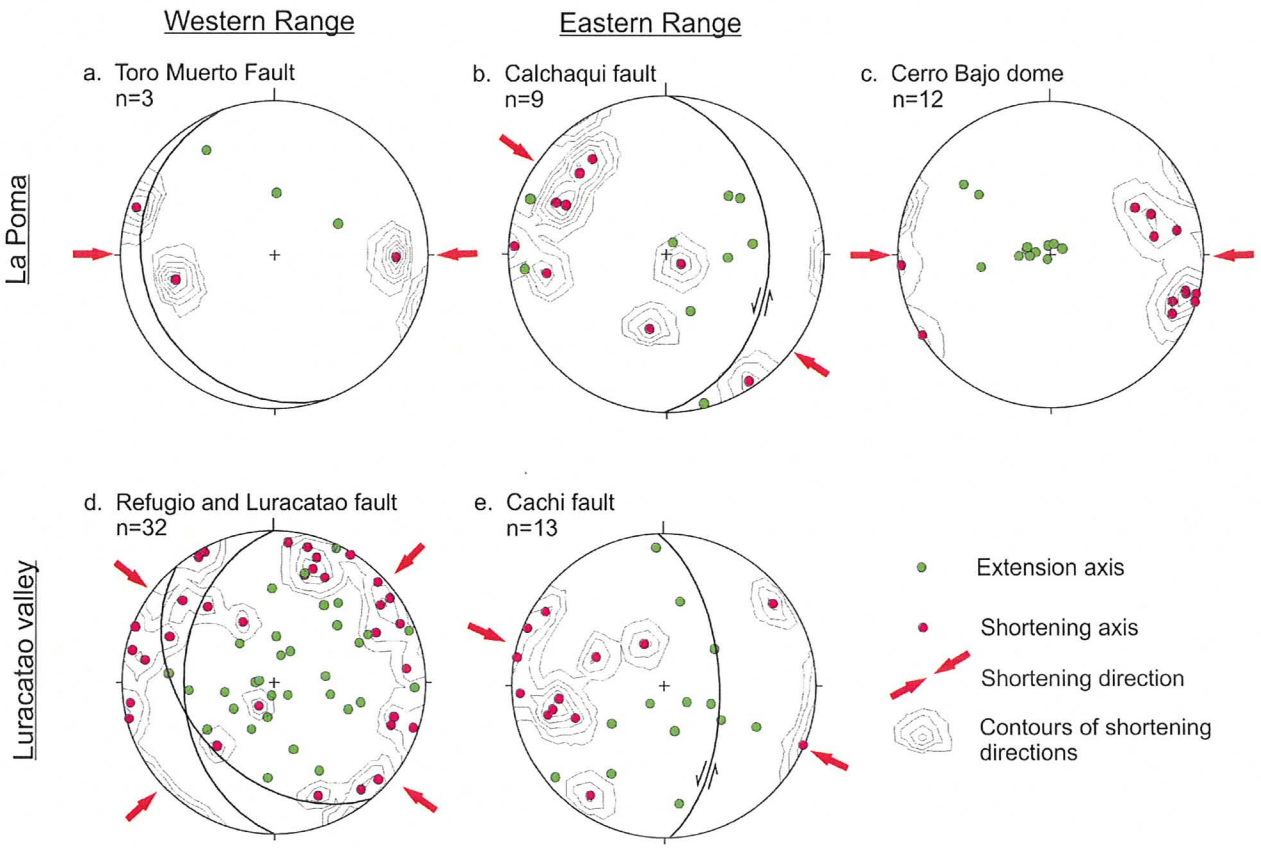

Figure 13- Lower-hemisphere equal-area projection showing shortening and extension directions for the La Poma area and Luracatao Valley. Great circles delineate the orientation of the fault plane.

Chapter 9: Significance of Structural Data

The formation of the Eastern Cordillera is a result of overall east-west shortening. As the Eastern Cordillera evolves, older structure, lithological difference and thrusting of basement rock determines the formation of structures. To assess the controlling factors associated with the evolution of the Eastern Cordillera knowedge of (1) the geometry of the first-order faults, (2) the orientation of local principal strain directions, (3) the sense of movement on a given fault plane and (4) pre-existing structural anisotropy is required. Lithological heterogeneity and climatic processes may also play an important role in the style of deformation and subsequent evolution of the regional landscape (Strecker et al., 2007).

9.1 Geometry of first-order faults

Although the location of first-order reverse faults at mountain fronts in the Eastern Cordillera is well known, the actual orientation of the respective fault planes has not been examined. This is important to understand the evolution of the basin and range morphology of the Eastern Cordillera. 3D modeling shows that the Toro Muerto Fault dips 10^{o}-15^{o} to the west and the Calchaquí Fault dips 25^{o}-35^{o} to the east in the La Poma area (Fig. 6). The fact that the Toro Muerto Fault dips shallowly and juxtaposes older rocks against younger rocks (Fig. 3, 4) indicates that it is a thrust fault. In the Luracatao Valley, the west-dipping Refugio Fault and east-dipping Cachi Fault have respectively an average dip of 40^{o} and 60^{o} (Fig. 10). Therefore, the orientation of the west-dipping faults is shallower than the east-dipping faults in both areas.

The relationship between the geometry of the shallower west-dipping and steeper east-dipping faults can be mechanically explained. As deformation in the Central Andes propagates from west to east (Deeken et al., 2006), it is mechanically easier to displace rocks on west-dipping thrust faults than on steep reverse faults. This can explain why the west-dipping Toro Muerto Fault in the LaPoma area developed as a thrust fault in contrast to the east-dipping Calchaquí Fault, which may act as a back thrust with regard to eastward propagating deformation. As displacement on the thrust fault continues, displaced rock mass increases the load on the fault, thus locking the fault and temporarily terminating movement on the fault. To accommodate shortening during such fault locking, displacement is transferred to an east-dipping reverse fault serving as a back thrust. This may be the reason why the Toro Muerto Fault does not show evidence of activity in Quaternary times, in contrast to the Calchaquí Fault (Guzmán et al. 2006), and is, therefore, likely older than the Calchaquí Fault.

The dip of a fault may also be controlled by the pre-existing anisotropy in the rock. This is evident in the Luracatao Valley where the orientation of the Refugio Fault plane is concordant to the metamorphic foliation in meta-granitoid rocks (Fig. 12e, f). This may explain why the Refugio Fault plane is steeper than the Toro Muerto Fault in the La Poma area. Like in this area, the east-dipping fault, i.e., the Cachi Fault, was active during Quaternary times (Fig. 12 a, b). In fact, Quaternary deformation is also evident on the east-dipping reverse fault in the Cachi area. In addition, the dip of the Cachi Fault can be attributed to pre-existing activity of this fault as a normal fault in Cenozoic times, i.e., before reactivation as a reverse fault (e.g., Hongn and Seggiaro, 2001; Riller and Hongn, 2003; Carrera et al., 2006).

9.2 Paleo-stress directions near first-order structures

In order to better understand the kinematics of deformation, the directions of principal paleo-stresses, which are interpreted in terms of paleo-strain directions in this study, were identified near first-order structures. In the La Poma area, the Cerro Bajo Dome and the Toro Muerto Fault are characterized by subhorizontal E-W shortening and subvertical extension (Fig. 13). By contrast, NW-SE shortening directions are more prominent at the east-dipping Calchaquí Fault. Therefore, this fault has a left-lateral component of displacement in addition to the reverse sense of slip. Similarly, NW-SE shortening directions are evident at the east-dipping Cachi Fault in the Luracatao Valley indicating a left-lateral displacement component on this fault as well. Thus the east-dipping reverse faults in both valleys are characterized by a component of left-lateral displacement.

In contrast to the uniform shortening directions associated with the east-dipping faults in both valleys, the Refugio Fault and Luracatao Fault show NW-SE and NE-SW directions of shortening (Fig. 13). Therefore, the Refugio Fault shows two events of deformation while the uniform NW-SE shortening near east-dipping faults in both valleys attests to a single deformation event. Since displacement on the east-dipping faults lasted until Quaternary times, NE-SW shortening associated with the Refugio Fault represents likely an older deformation event. It is thus conceivable that the Refugio Fault has undergone a longer deformation history than the east-dipping reverse faults.

Brittle fault planes of the Cerro Bajo Dome are mostly concordant to east-dipping bedding planes in the mechanically competent carbonate layers of the Yacoraite Formation (Fig. 3, Appendix A 1) and sandstone of the Tertiary strata. Therefore, the Dome formed by the process of flexural slip on the bedding surfaces. As slip on the bedding planes was achieved by E-W shortening (Fig. 13), non-cylindrical deformation (doming) occurred under overall E-W shortening.

Although regional shortening in the Eastern Cordillera is E-W, the shortening directions vary with location and the local deformation regime (thrusting, reverse faulting, doming) in the study areas. This suggests, that the orientation of local paleo-stress (strain) directions is controlled by the local configuration of prominent structures and, therefore, cannot ad hoc be interpreted in terms of the far field stresses resolved by absolute plate motion (e.g., plate convergence direction).

9.3 Style of deformation in the Eastern Cordillera

Deformation in the Eastern Cordillera initiated with non-cylindrical deformation (doming) associated with E-W shortening as seen in the La Poma area. This stage of deformation was followed by cylindrical deformation evident by rather straight first-order faults that intersect the Cerro Bajo Dome (Fig.3, 14). Straight first-order reverse faults are also observed in the Luracatao Valley and the Cachi area. The shortening directions on the west-dipping Refugio Fault in this valley are NW-SE and NE-SW (Fig. 13d, 14). By contrast, the east-dipping reverse faults in all three study areas show NW-SE shortening direction (Fig. 11, 13b, e) and occurred in Quaternary times. Thus, cylindrical deformation likely started in Tertiary times under NE-SW shortening and continued into Quaternary times under NW-SE shortening that included a left-

lateral component of displacement on the N-S striking reverse faults. The fact that cylindrical deformation (doming) occurred under E-W shortening and preceded cylindrical deformation (thrusting and reverse faulting), corroborates the notion that shortening directions in the Eastern Cordillera vary with time and position and therefore, cannot be reliably used as indicators for the orientation of principal far-field stresses.

The Cerro Bajo dome and first-order faults in the La Poma area show morphological similarities to the Cachi area together with the Cerro Tintin Dome (Fig. 1c). As in La Poma, the Cachi area also displays non-cylindrical deformation by the formation of the Cerro Tintin and cylindrical deformation visible in the Quaternary strata of this area. Therefore, localized domes or non-cylindrical deformation in the Eastern Cordillera and Plateau may be the initial response of the upper crust to horizontal shortening. Doming may be due to local structural and/or mechanical anisotropy in basement rocks, which is followed by cylindrical deformation manifested by straight thrust and reverse faults as horizontal shortening progresses.

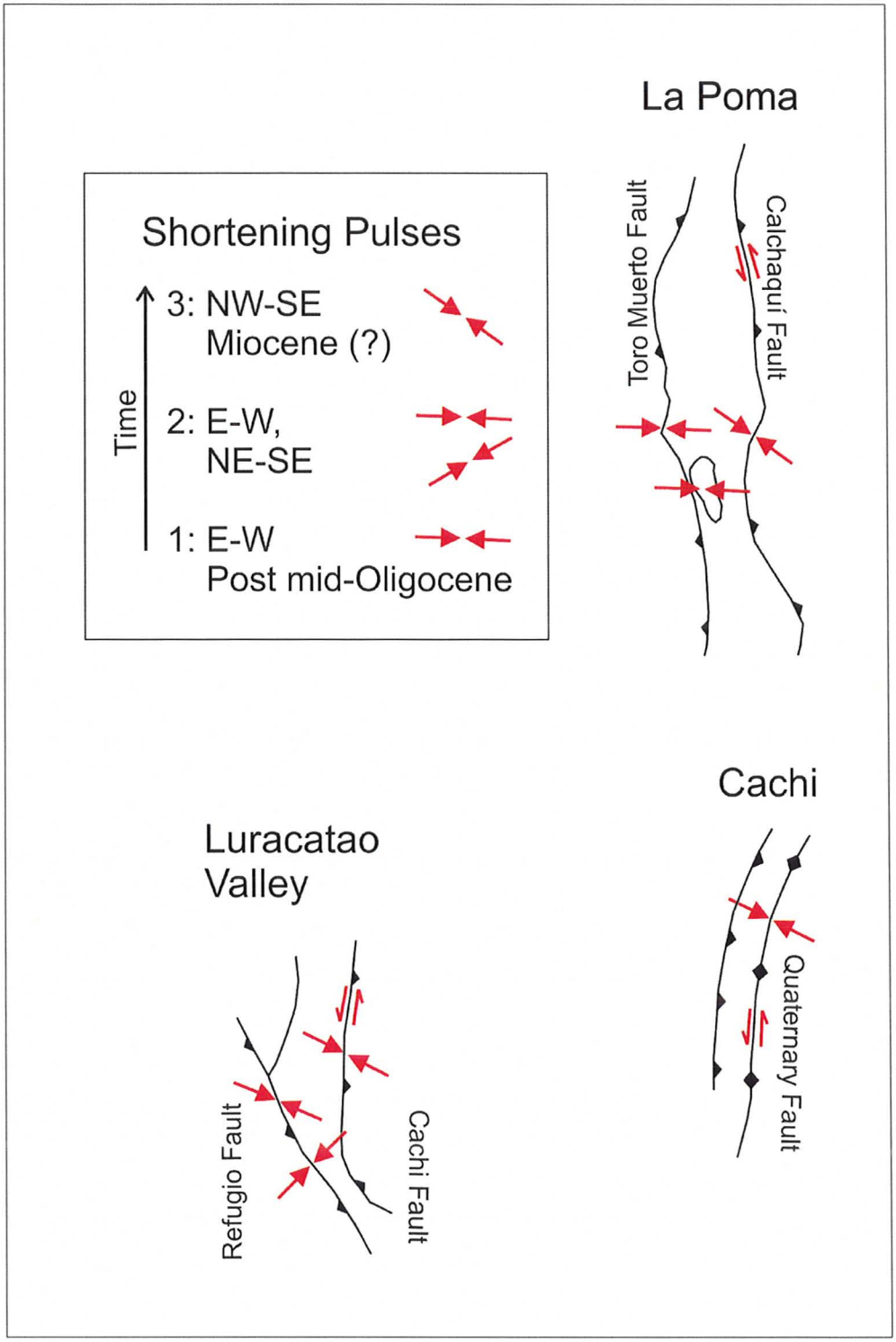

Figure 14- Simplified map delineating the style and timing of deformation in the Eastern Cordillera.

Chapter 10: Conclusions

The structural study of the Calchaquí Valley and the Luracatao Valley has provided an insight into the kinematics and mechanisms of deformation in the Eastern Cordillera. The analysis of fault geometry and fault-slip data provides a history of deformation events that reveals two stages of distinct deformation regimes. Deformation starts with local doming of upper crust (non-cylindrical deformation) that may be due to localized anisotropy (mechanical instabilities) in the basement rocks. Doming is followed by the formation of N-S striking reverse faults (cylindrical deformation), which forms the valley and range morphology that is typical for the Eastern Cordillera and the Puna Plateau. As Andean deformation propagated from west to east in Tertiary times, shortening was first accomplished on west-dipping thrust and reverse faults in the Luracatao Valley and the Calchaquí Valley, respectively. Toward Quaternary times, shortening is achieved on east-dipping reverse faults, which served likely as back thrusts to west-dipping faults. This can explain why Quaternary deformation is only evident on the eastern ranges of the Calchaquí Valley and Luracatao Valley. Analysis of brittle shear faults indicates that doming occurred during E-W shortening. This was followed by NE-SW-shortening on west-dipping thrust and reverse faults and later by NW-SE shortening on east-dipping reverse faults, which induced also a component of left-lateral displacement on N-S striking reverse faults. Brittle fault analysis indicates that shortening directions vary greatly in space and time and seem to depend rather on the local kinematic regime of first-order deformation mechanisms (doming, thrusting, reverse faulting) than on far-field stresses related to plate boundary forces.

Appendix A- Lower-hemisphere equal-area projections of the fault-slip data

Calchaquí Fault- Calchaquí Valley

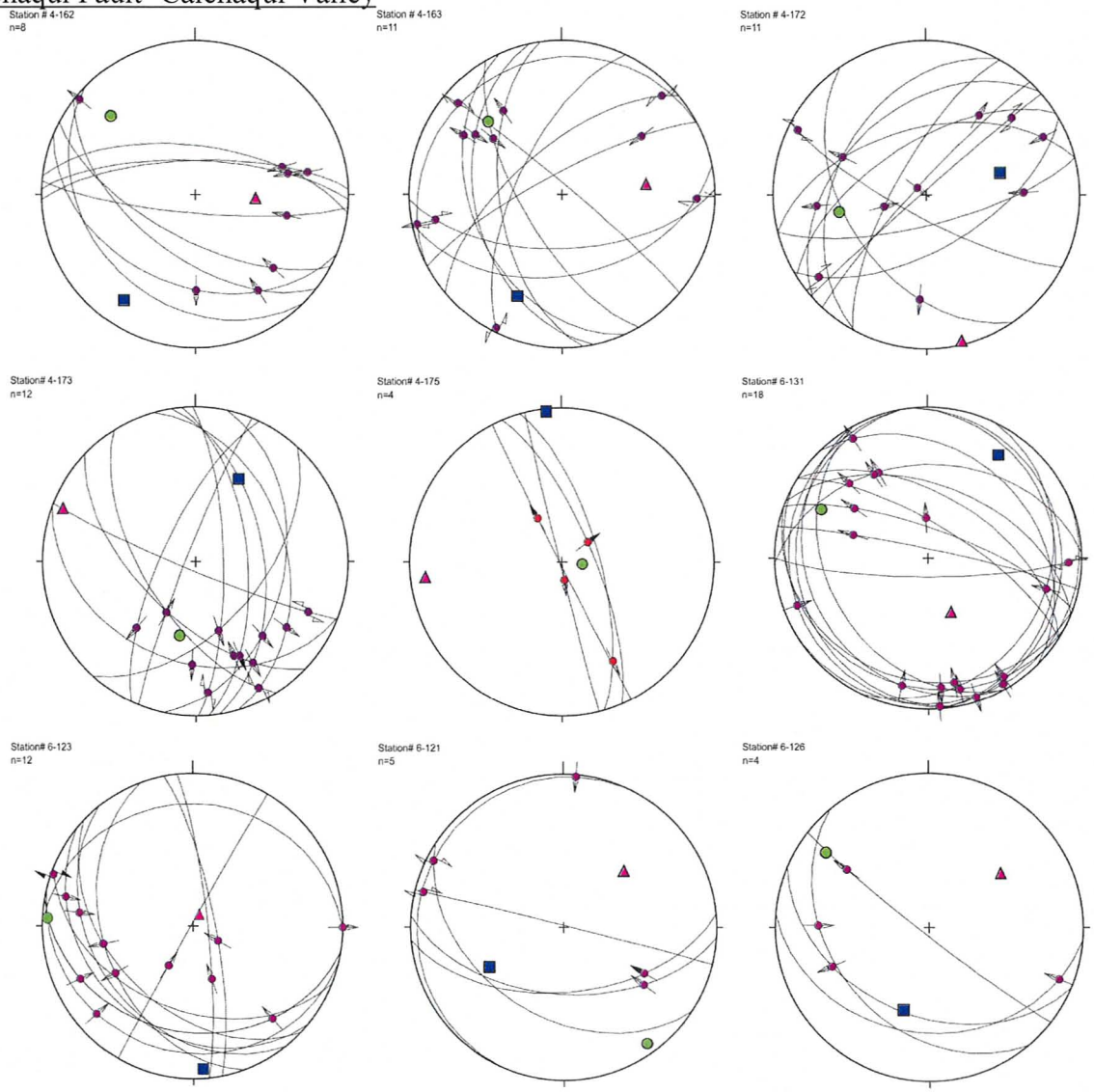

Toro Muerto Fault-Calchaquí Valley

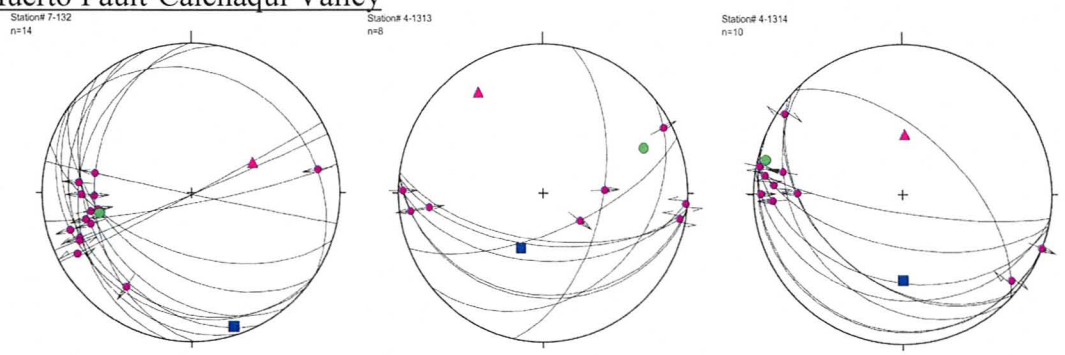

Cerro Bajo Dome- Calchaquí Fault

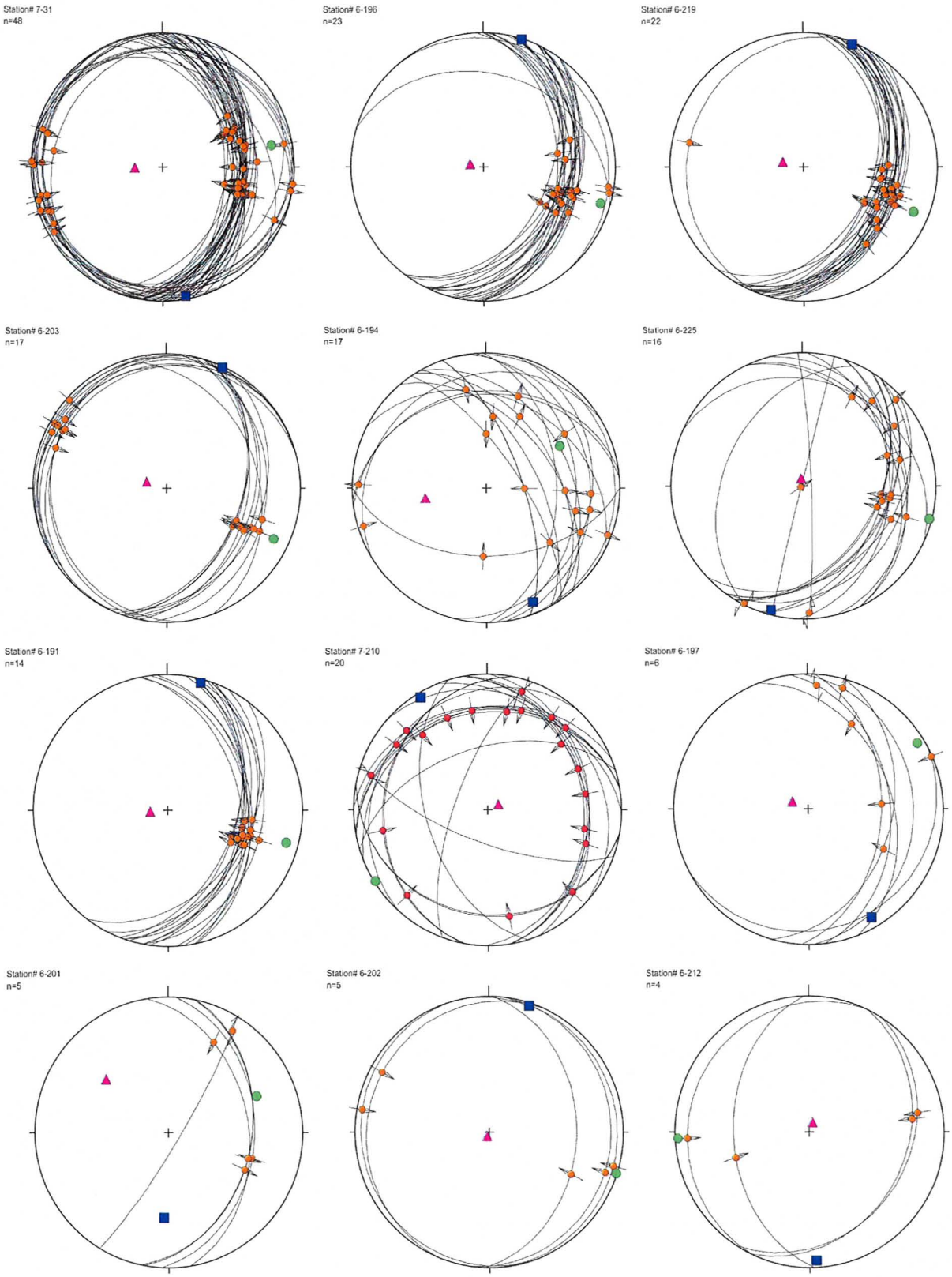

Cachi Fault-Luracatao Valley

Station# 7-181
n=7

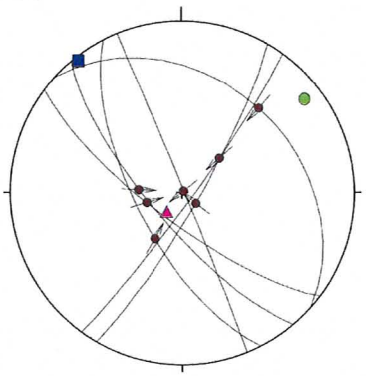

Station# 3-141
n=23

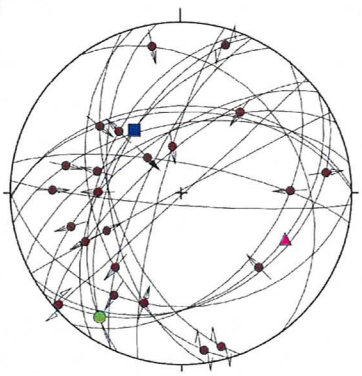

Station# 3-163
n=16

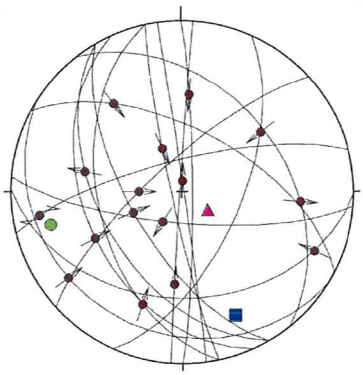

Station# 3-168
n=15

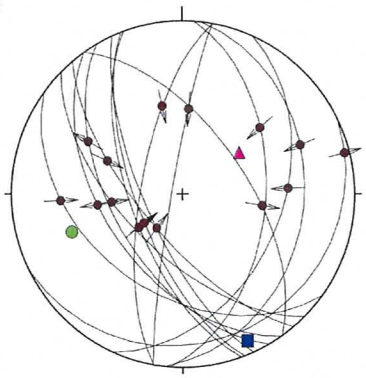

Station# 5-32
n=19

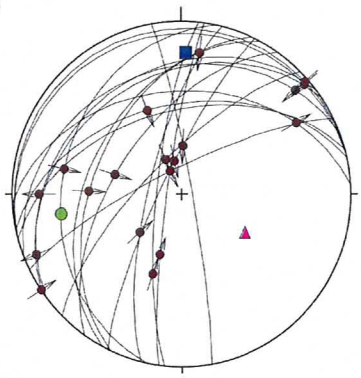

Station# 5-35
n=12

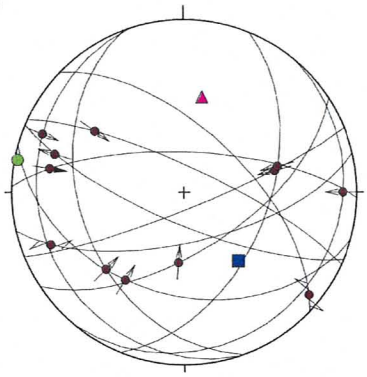

Staiton# 5-36
n=7

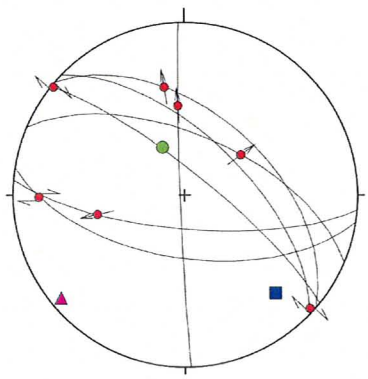

Station# 5-37
n= 14

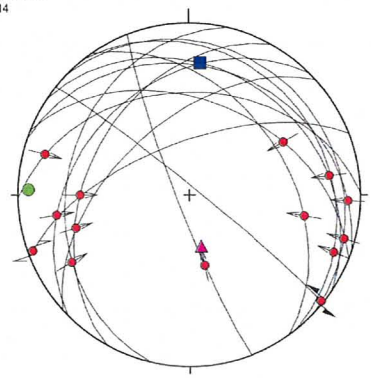

Station# 5-38
n=13

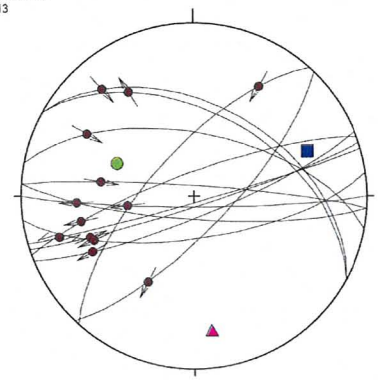

Station 5-39
n=25

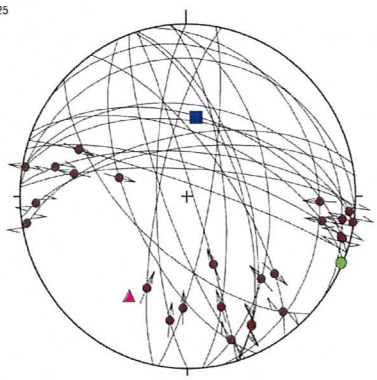

Station# 5-42
n=6

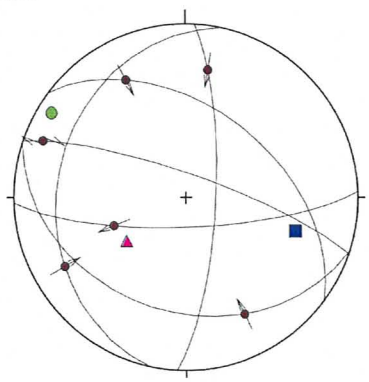

Station# 5-46
n=11

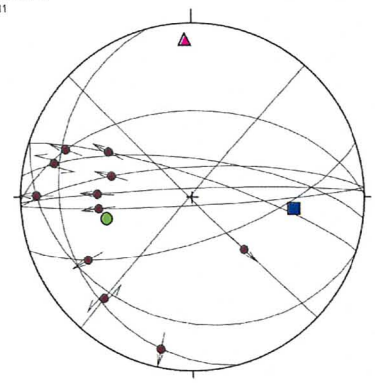

Refugio Fault- Luracatao Valley

Station# 7-251
n=22

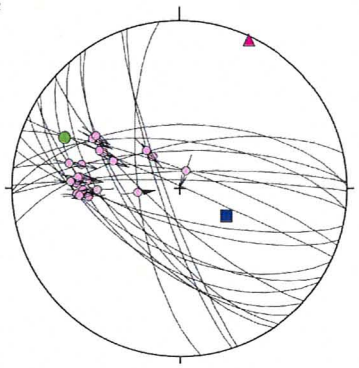

Station# 4-281
n=6

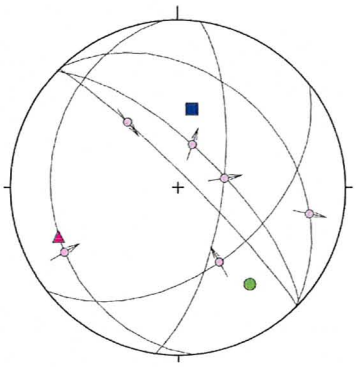

Station# 4-282
n=9

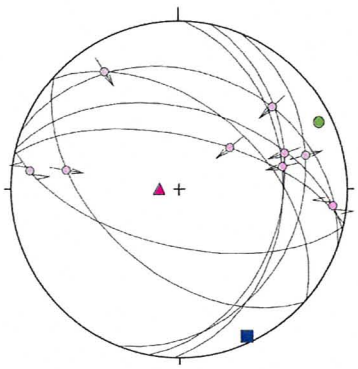

Station# 4-285
n=5

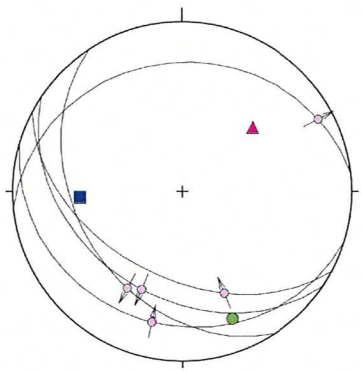

Station# 4-289
n=5

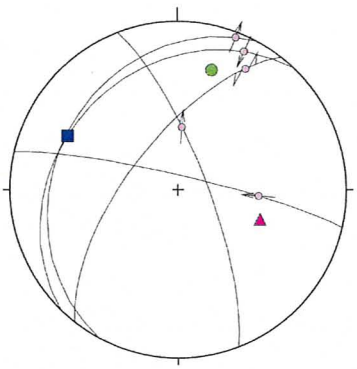

Station# 4-2810
n=13

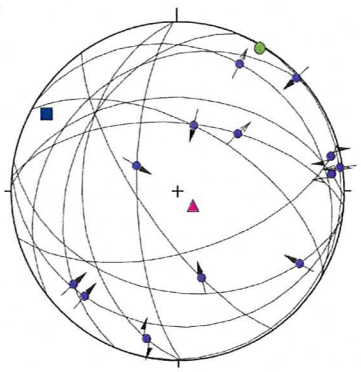

Station# 4-2818
n=5

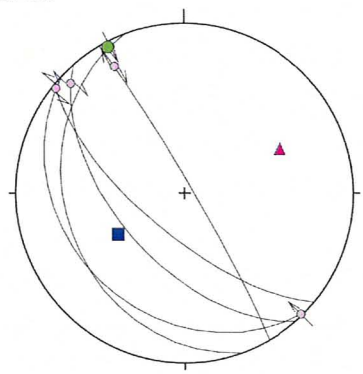

Station# 4-2819
n=8

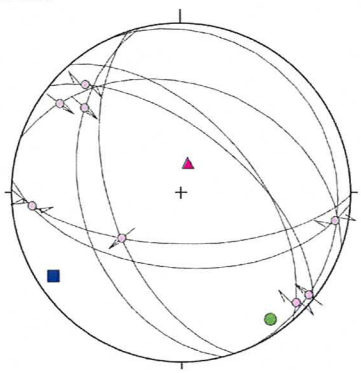

Station# 4-2820
n=14

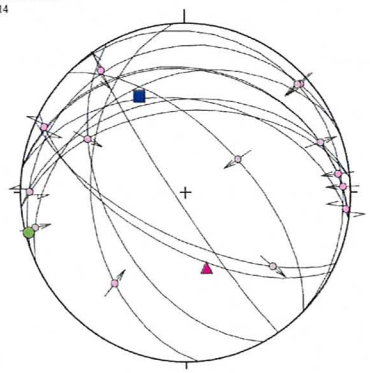

Station# 4-2821
n=8

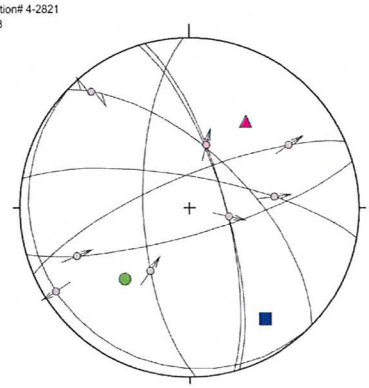

Station# 4-295
n=8

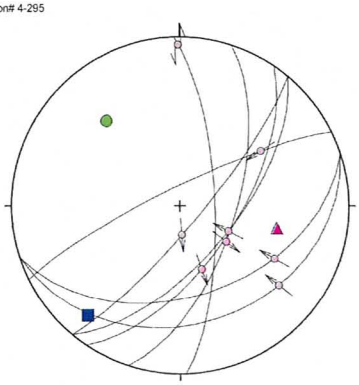

Station# 4-296
n=6

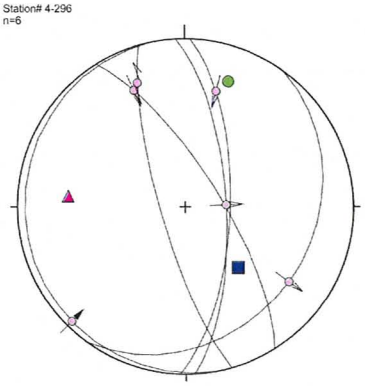

Refugio Fault-Luracatao Valley (cont'd)

Station# 5-296 (b)
n=9

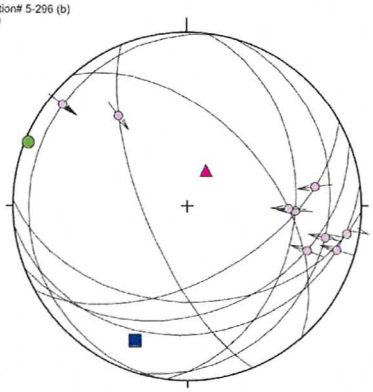

Station# 4-2913
n=7

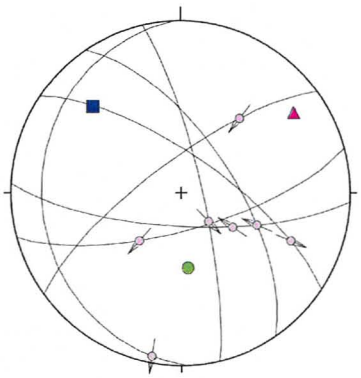

Station# 4-2917
n=11

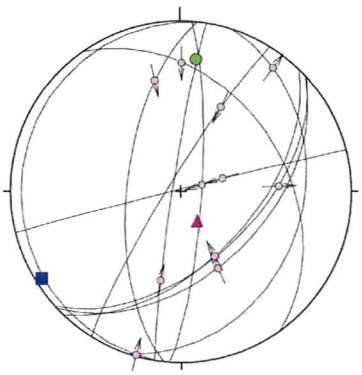

Station# 4-2918
n=5

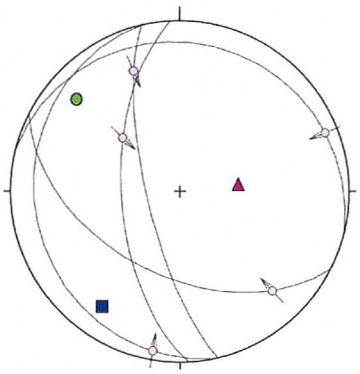

Station# 4-2919
n=5

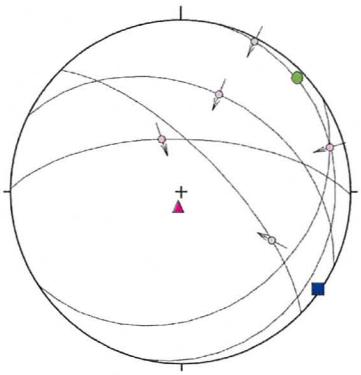

Station# 4-2920
n=6

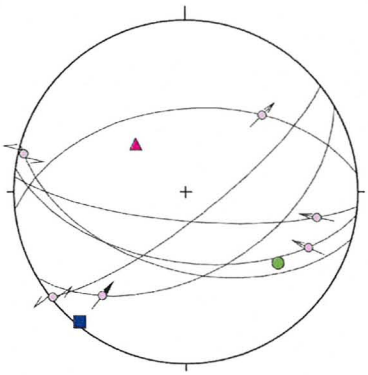

Station# 4-308
n=7

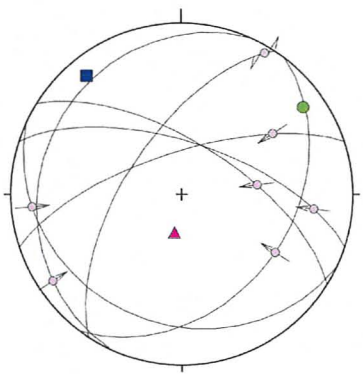

Station# 4-3015
n=14

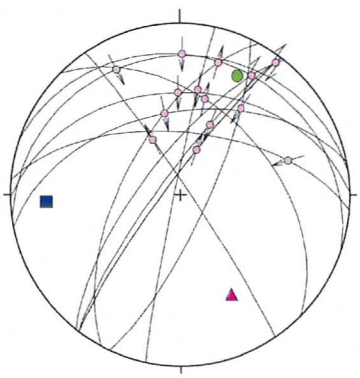

Station# 4-3019
n=18

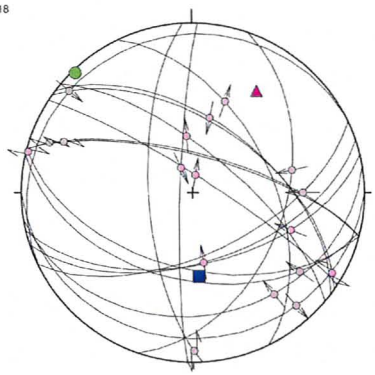

Station# 5-11
n=6

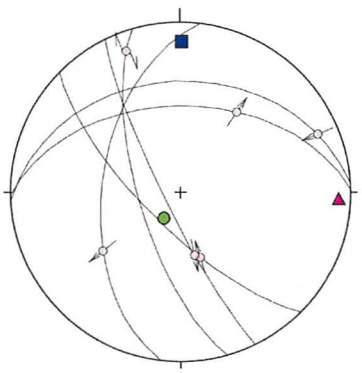

Station# 5-13
n=5

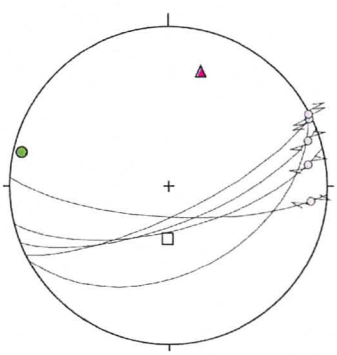

Station# 5-13
n=7

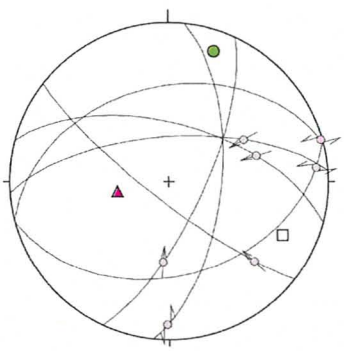

Refugio Fault-Luracatao Valley (cont'd)

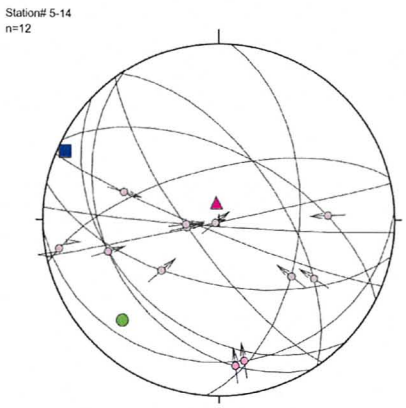

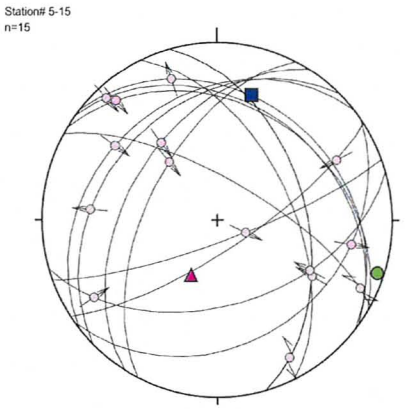

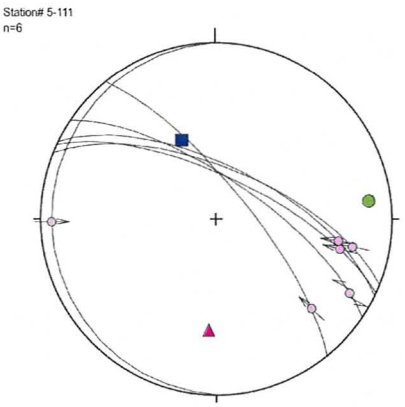

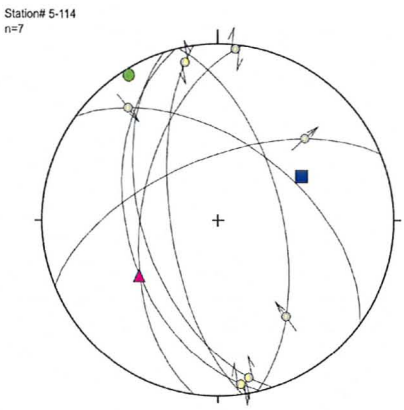

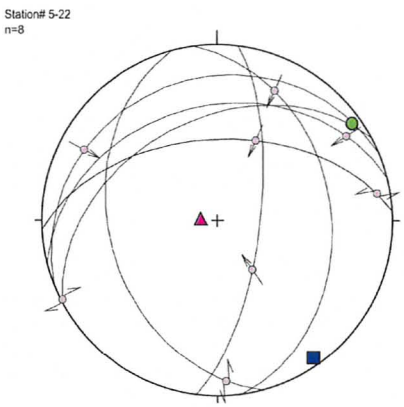

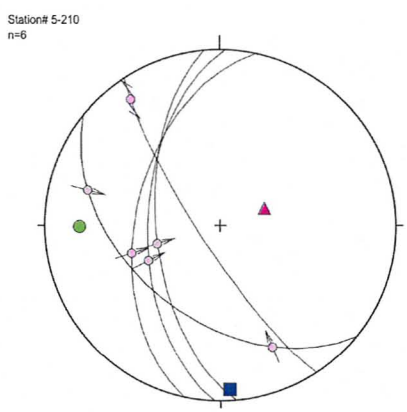

Luracatao Fault

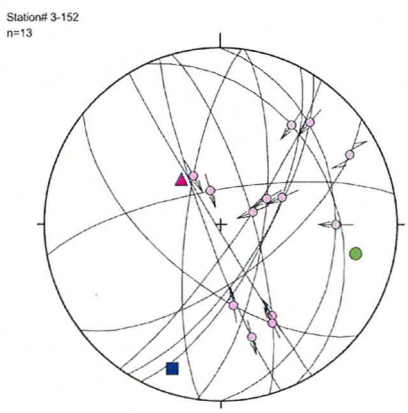

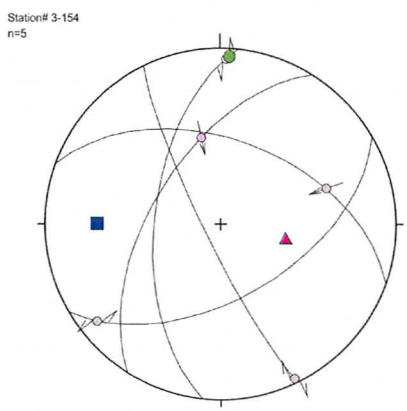

Legend

- Maximum principal axis
- Intermediate principal axis
- Minimum principal Axis
- Breccia zones
- Apilitic dykes
- Mealla Formation
- Yacoraite Formation
- Complejo Eruptivo Oire
- Pirugua Formation
- Puncoviscana Formation

References

Allmendinger, R.W., Jordan, T.E., Kay, S.M., and Isacks, B.L., 1997, the evolution of the Altiplano-Puna Plateau of the Central Andes. Annual Review of Earth and Planetary Sciences, v. 25, p. 139-174.

Alonso R.N., Jordan T.E., Tabbutt, K.T., Vandervoort, D.S., 1991. Giant evaporate belts of the Neogene central Andes. Geology. 19 (4): 401-404.

Angelier, J., Goguel, J., 1979. Su rune methode dimple de determination des axes princepaux des contraintes pour une polulation de failles. Comptes Randus Hebdomadaires des Seacnes de l'Academie des Sciences, Serie D: Sciences Naturelles 288 (2): 307-310.

Baldis, B., Gorroño, A., Ploskiewicz, J. And Sarudiansky, R., 1976. Geotectónica de la Cordillera Oriental, Sierras Subandinas y comarcas adyaccentes. Actas 6 Congreso Geológico Argentino, 1: 3-22. Buenos Aires.

Blasco, G., Zapettini, E., 1995. Geología. In Blasco, G., E. Zapettini and F. Hongn; Hojo Geológica San Antonio de los Cobres (Mapa), Escala 1:250,000. Secretaría de Minería de la Nación, Dirección Nacional del Servicio Geológico. Buenos Aires.

Bookhagen, B., Strecker, M.R., 2008. Orographic barriers, high resolution TRMM rainfall, and relief variations along the eastern Andes. Geophysical Research letters. 35 (6).

Bosio, P.P., Powell, J., Del Papa, C., Hongn, F., 2009. Middle Eocene deformation-sedimentation in the Luracatao Valley: Tracking the beginning of the foreland basin of northwestern Argentina. Journal of South American Earth Science. 28: 142-154

Byerlee, J.D., 1968. Brittle-ductile transition in rocks. Journal of Geophysical Research 73 (14): 4741-4750

Carrera, N., Muñoz, J.A., Sábat, F., Mon, R., Roca, E., 2006. The role of inversion tectonics in the structure of the Cordillera Oriental (NW Argentinean Andes). Journal of Structural Geology 1, 12.

Coward, M. P., Potts, G.J., Complex strain patterns developed at the frontal and lateral tips to shear zones and thrust zones. Journal of Structural Geology. 5 (3-4): 383-399

DeCelles, P., Horton, B.K., 2003. Early to middle Tertiary foreland basin development and the history of Andean crustal shortening in Bolivia. Geological Society of America Bulletin. 115: 58-77

Deeken, A., Sobel, E.R., Coutand, I., Haschke, M., Riller, U., Strecker, M.R., 2006. Development of the southern Eastern Cordillera, N.W. Argentina, constrained by apatite fission

track thermochronology: From Early Cretaceous extension to middle Miocene shortening, Tectonics. 25.

Díaz, J., Malizzia, D., Bossi, G., 1987. Análisis estratigráfico del Grupo Payogastilla (Terciario Sup.) X Congreso Geológico Argentino, II, 113-117.

Gephart, J., 1994. Topography and subduction geometry in the central Andes: clues to the mechanics of a non-collisional orogen. Journal of Geophysical Research. 99:12, 279-12, 288.

Guzmán, S.R., Petrinovic, I.A., Brod, J.A., 2006. Pleistocene mafic volcanoes in the Puna-Cordillera Oriental boundary, NW-Argentina. Journal of Volcanology and Geothermal Research. 158: 51-69

Hongn, F., Seggiaro, R.E. 2001. Hoja Geológica 2566-III, Cachi, 1:250 000. Mapa geológico y capítula Tectónica (p.53-65). SEGEMAR. Boletín 248. Buenos Aires.

Hongn, F., del Papa, C., Powell, J., Petrinovic, I., Mon, R., Deraco, V., 2007. Middle Eocene deformation and sedimentation in the Puna-Eastern Cordillera transition (23°-26°S): Control by pre-existing heterogeneities on the pattern of initial Andean shortening. Geology. 35 (3): 271-274.

Hongn, F.D., Riller, U. 2007. Tectonic evolution of the western margin of Gondwana inferred from syntectonic emplacement of paleozoic granitoid plutons in N.W. Argentina. Journal of Geology. 115(2): 163-180.

Isacks, B.L., 1988. Uplift of the central Andean Plateau and bending of the Bolivian Orocline. Journal of Geophysical Research, 93: 3211-3231.

Kley, J., 1996. Transition from basement-involved to thin-skinned thrusting in the Cordillera Oriental of southern Bolivia, Tectonics, 15: 763-775.

Kley, J., Gangui, A.H., and, Krüger, D., 1996. Basement-involved blind thrusting in the eastern Cordillera Oriental, southern Bolivia: Evidence from cross-sectional balancing, gravimetric and magnetotelluric data, Tectonophysics, 259: 171-184

Kley, J., Müller, J., Tawackoli, S., Jacobshagen, V., Manutsoglu, E., 1997. Pre-Andean and Andean-age deformation in the Eastern Cordillera of Southern Bolivia. Journal of South Amercian Earth Science, 10: 1-19.

Marrett R.A., Allmendinger R.W., Alonso R.N., 1994. Late Cenozoic tectonic evolution of the Puna Plateau and adjacent foreland, northwestern Argentine Andes. Journal of South American Earth Science 7:179-207

Marrett, R., Strecker, M.R., 2000. Response of intercontinental deformation in the central Andes to the late Cenozoic reorganization of South American plate motions. Tectonics. 19:452-467.

Mon, R., and J.A. Salfity., 1995. Tectonic evolution of the Andes of northern Argentina, in Petroleum Basins of South America, edited by A.J. Tankard, R. Suáres, and H.J. Welsink, AAPG Mem., 62: 269-283.

Moreno, J.A., 1970. Estratigrafía y Paleogeografía del Cretácico superior en la cuenca del Noroeste Argentine, con especial mención de los subgrupos Balbuena y Santa Bárbara. Revista de la Asociación Geológica Argentina. 24: 9-44.

Oncken, O., Hindle, D., Kley, J., Elger, K., Victor, P., Schemmann, K. 2006. Deformation of the Central Andean upper plate system-facts, fiction and constraints for plateau models. In: O.Oncken, G. Chong, G. Franz, P. Giese, H.J. Götze, V. Ramos, M. Strecker, and P. Wigger (eds.): The Andes. Active subduction orogeny, Frontiers in Earth Sciences 1, Springer, Berlin, p. 3-27.

Petrinovic, I.A., Riller, U., Brod, A., 2005. The Negra Muerta Complex, southern Central Andes: geochemical characteristics and magmatic evolution of an episodically active volcanic center. Journal of Volcanology and Geothermal Reasearch 140: 205-320

Riller, U., Greskowiak, J., Ramelow, J. & Strecker, M. 1999. Dominant modes of Andean deformation in the Calchaquí River Valley, NW-Argentina. XIV Argentine Geological Congress, Actas I, Salta. p. 201-204.

Riller, U., Petrinovic, I., Ramelow, J., Strecker, M., Oncken, O., 2001. Late Cenozoic tectonism, collapse caldera and plateau formation in the central Andes. Earth and Planetary Science Letters. 188: 299-311.

Riller, U. and Hongn, F., 2003. Structural significance of Paleozoic discontinuities on Cretaceous to Quaternary tectonism in the eastern Cordillera, NW-Argentina. Geophysical Research Abstracts, Volume 5, 02303.

Riller, U., Oncken O., 2003 Growth of the Central Andean plateau by tectonic segmentation is controlled by the gradient in crustal shortening. Journal of Geology. 1111: 367-384.

Salfity, J.A., 2008. Geología regional del Valle Calchaquí, Argentina. Boletín Academia Nacional de Ciencias, Córdoba

Spang, J.H., 1972. Numerical method for dynamic analysis of calcite twin lamellae. Geological Society of America Bulletin 83 (2), 467-471.

Sperner, B., Ratschbacher, L., 1994. A Turbo Pascal program package for graphical presentation and stress analysis of calcite deformation. Seitschrift der Deutschen Geologischen Gesellschaft 145: 414-423.

Sperner, B., Ratschbacher, L., Ott, R., 1993. Fault-striae analysis; a Turbo Pascal program package for graphical presentation and reduced stress tensor calculations. Computers & Geosciences 19 (9): 1361-1388.

Sperner, B. and Zweigel, P., 2010. A plea for more caution in fault–slip analysis. Tectonophysics 482: 29-41.

Strecker, M.R., Alonso, R.N., Bookhagen, B., Carrapa, B., Hilley, G.H., Sobel, E.R., Trauth, M.R., 2007. Tectonics and climate of the southern central Andes, Annual Review of Earth and Planetary Sciences. Sc., 35: 747-787

Turner, F.J., 1953. Nature and dynamic interpretation of deformation lamellae in calcite of three marbles. American Journal of Science 251: 276–298.

Turner, J.C.M., 1959. Estratigrafía del cordon de escaya y de la sierra de Rinconada (Jujuy), Rev. Asoc. Geol. Argent., 13: 15-39.

Turner, J.C. 1960. Estratigrafía de la Sierra de Santa Victoria y adyacencias. Bol. Acad. Ciences. Cordoba 41:163-196

Turner, J.C.M. 1960. Estratigrafía de Nevado de Cachi y sector al oeste (Salta); Acta Liliona III, pp. 191-226.

Vandervoort, D.S., T.E. Jordan, P.K. Zeitler, and R.N. Alonso, 1995. Chronology of internal drainage development and uplift, southern Puna plateau, Argentine central Andes, Geology, 23, 145-148

Viramonte, J.G., Omarini, R.H., Araña Saavedra V., Aparicio A., Garcia Cacho, L, Parica, P., 1984. Edad, genesis y mecanismos de erupcion de las riolitas granatiferas de San Antonio de los Cobres, Provincia de Salta, IX. Congreso Geológico Argentino. Actas III: 216-233.